Toward explaining the Holocene carbon dioxide and carbon isotope records: Results from transient ocean carbon cycle-climate simulations

L. Menviel[1,2] and F. Joos[1,2]

Received 6 September 2011; revised 9 November 2011; accepted 28 November 2011; published 14 February 2012.

[1] The Bern3D model was applied to quantify the mechanisms of carbon cycle changes during the Holocene (last 11,000 years). We rely on scenarios from the literature to prescribe the evolution of shallow water carbonate deposition and of land carbon inventory changes over the glacial termination (18,000 to 11,000 years ago) and the Holocene and modify these scenarios within uncertainties. Model results are consistent with Holocene records of atmospheric CO_2 and $\delta^{13}C$ as well as the spatiotemporal evolution of $\delta^{13}C$ and carbonate ion concentration in the deep sea. Deposition of shallow water carbonate, carbonate compensation of land uptake during the glacial termination, land carbon uptake and release during the Holocene, and the response of the ocean-sediment system to marine changes during the termination contribute roughly equally to the reconstructed late Holocene pCO_2 rise of 20 ppmv. The 5 ppmv early Holocene pCO_2 decrease reflects terrestrial uptake largely compensated by carbonate deposition and ocean sediment responses. Additional small contributions arise from Holocene changes in sea surface temperature, ocean circulation, and export productivity. The Holocene pCO_2 variations result from the subtle balance of forcings and processes acting on different timescales and partly in opposite direction as well as from memory effects associated with changes occurring during the termination. Different interglacial periods with different forcing histories are thus expected to yield different pCO_2 evolutions as documented by ice cores.

Citation: Menviel, L., and F. Joos (2012), Toward explaining the Holocene carbon dioxide and carbon isotope records: Results from transient ocean carbon cycle-climate simulations, *Paleoceanography*, *27*, PA1207, doi:10.1029/2011PA002224.

1. Introduction

[2] The Holocene is the last warm period of the glacial/interglacial cycles that characterize the climate over the past million years [*Jansen et al.*, 2007]. Reconstructions of atmospheric CO_2 (pCO_2) [*Indermühle et al.*, 1999; *Monnin et al.*, 2001] based on Antarctic ice cores reveal significant and well quantified variations over this current interglacial. Atmospheric CO_2 decreased by about 5 ppmv in the early Holocene (11,000 to 7,000 years before present (11 to 7 ka B.P.)) and increased by 20 ppmv during the late Holocene before the recent, much larger and faster anthropogenic pCO_2 rise. The Holocene variations are also relatively small compared to the glacial/interglacial range of 170 to 300 ppmv of the last 800,000 years (800 kyr) [*Lüthi et al.*, 2008].

[3] The goals of this study are (1) to investigate and quantify the mechanisms involved in the Holocene carbon cycle changes with the Bern3D Earth System Model of Intermediate Complexity, (2) to test the robustness of the results obtained with the mass balance approach by *Elsig et al.* [2009], and (3) to further constrain the magnitude of land carbon uptake and release during the last deglaciation and the Holocene. A multiproxy approach is invoked and the intention is to simultaneously reproduce records of atmospheric CO_2 and $\delta^{13}C$ as well as the spatiotemporal evolution of $\delta^{13}C$ of dissolved inorganic carbon ($\delta^{13}C_{DIC}$) [e.g., *Oliver et al.*, 2010] and carbonate ion concentration ($[CO_3^{2-}]$) in the deep sea [*Yu et al.*, 2010a, 2010b]. Marine processes considered here include calcium carbonate compensation of terrestrial carbon uptake and release, shallow-water carbonate deposition, changes in sea surface temperature (SST), ocean circulation, marine productivity and related ocean-sediment interactions in response to glacial/interglacial reorganizations. We rely on scenarios from the literature to prescribe the evolution of shallow-water carbonate deposition [*Milliman*, 1993; *Kleypas*, 1997; *Vecsei and Berger*, 2004] and of land carbon stock changes [*Elsig et al.*, 2009; *Yu et al.*, 2010; *Menviel et al.*, 2011] and modify these scenarios within uncertainties. The focus of this study is on marine processes and we do not model terrestrial carbon changes explicitly nor do we address terrestrial processes such as human land use changes [e.g., *Kaplan et al.*, 2010; *Stocker et al.*, 2011], but we do briefly assess

[1]Climate and Environmental Physics, Physics Institute, University of Bern, Bern, Switzerland.
[2]Oeschger Centre for Climate Change Research, University of Bern, Bern, Switzerland.

Copyright 2012 by the American Geophysical Union.
0883-8305/12/2011PA002224

source: https://doi.org/10.7892/boris.18174 | downloaded: 24.4.2024

which net terrestrial stock changes are consistent with the available information.

[4] *Broecker et al.* [2001] detail how land carbon uptake during the last deglaciation (18 to 11 ka B.P.), or in the early Holocene, causes a long-term, multimillennial adjustment of the calcium carbonate ($CaCO_3$) cycle that forces pCO_2 to rise. The timescale of this carbonate compensation mechanism is of the order of 5000 years [*Broecker and Peng*, 1987; *Keir*, 1988; *Archer et al.*, 1997; *Tschumi et al.*, 2011]. The mechanism works as follows: Terrestrial uptake depletes atmospheric CO_2 and through air-sea gas exchange the oceanic content of dissolved inorganic carbon (DIC = $[CO_2]$ + $[HCO_3^-]$ + $[CO_3^{2-}]$), whereas the alkalinity is unaffected by air-sea exchange. As a result, $[CO_3^{2-}]$ increases despite the DIC decrease, which leads to a better preservation of $CaCO_3$ in sediments. The calcite saturation horizon and the lysocline temporary deepen inducing enhanced $CaCO_3$ burial. The precipitation of $CaCO_3$ can be approximatively described by the following net equation:

$$Ca^{2+} + 2HCO_3^- = CaCO_3 + CO_2 + H_2O \quad (1)$$

Assuming the weathering input of DIC and alkalinity to the ocean has not changed, the enhanced $CaCO_3$ precipitation causes a DIC and alkalinity decrease in the ocean in a 1:2 ratio, and an increase in the ocean partial pressure of CO_2. As a result, the atmospheric CO_2 increases. The carbonate compensation mechanism does not have a significant impact on atmospheric $\delta^{13}C$ [*Tschumi et al.*, 2011], nor does it explain the CO_2 rise during the glacial termination (18–11 ka B.P.).

[5] Complementary, it is suggested that an increase in carbonate deposition on shelves and in shallow-waters [*Keir and Berger*, 1985; *Milliman*, 1993; *Walker and Opdyke*, 1995; *Kleypas*, 1997; *Opdyke*, 2000; *Vecsei and Berger*, 2004] contributed to the Holocene pCO_2 changes by up to 40 ppmv [*Ridgwell et al.*, 2003; *Kleinen et al.*, 2010]. Indeed, the net deposition of shallow-water carbonate leads to a release of CO_2. The disintegration of glacial ice sheets during the last glacial termination induced a sea level rise of about 120 m [*Fairbanks*, 1989; *Peltier*, 2004]. As the sea level rose, exposed continental shelves were flooded and the area of production of shallow-water carbonate increased. Available data on shelfal carbonate production during the deglaciation suggest that shallow-water carbonate production was strongest during the early Holocene (10–6 ka B.P.) [*Montaggioni*, 1988; *Ryan et al.*, 2001; *Spalding et al.*, 2001; *Vecsei and Berger*, 2004]. Uncertainties in the rate of shallow-water carbonate deposition are substantial and current estimates vary between 0.65 and 1.7 GtC/yr [*Milliman*, 1993; *Kleypas*, 1997; *Vecsei*, 2004].

[6] The Holocene pCO_2 variations provide a benchmark to challenge our mechanistic understanding of carbon cycle processes during warm periods. A range of studies attempted to quantitatively explain Holocene pCO_2 changes and contributing processes in the past 12 years [e.g, *Indermühle et al.*, 1999; *Broecker et al.*, 2001; *Brovkin et al.*, 2002; *Ridgwell et al.*, 2003; *Joos et al.*, 2004; *Schurgers et al.*, 2006; *Brovkin et al.*, 2008; *Kleinen et al.*, 2010; *Stocker et al.*, 2011]. These studies suffered, in general, from a lack of constraints to firmly attribute the reconstructed pCO_2 changes to individual terrestrial and marine mechanisms.

[7] Only recently a high quality record of the stable carbon isotope signature of atmospheric CO_2 ($\delta^{13}CO_2$) became available [*Elsig et al.*, 2009], providing a strong constraint on mechanisms. *Elsig et al.* [2009] used their data in a mass balance inversion with a reduced form model [*Joos and Bruno*, 1996] to quantify terrestrial and oceanic carbon fluxes. However, no mechanistic model simulations are, to our knowledge, yet available that explain simultaneously the atmospheric CO_2 and $\delta^{13}CO_2$ evolution presented by *Elsig et al.* [2009]. In addition, recent reconstructions of the spatiotemporal changes in deep $[CO_3^{2-}]$ [*Yu et al.*, 2010b, 2010a] and deep ocean $\delta^{13}C_{DIC}$ [*Carter et al.*, 2008; *McCave et al.*, 2008] provide additional benchmarks for our simulated results.

[8] A number of caveats apply to the mass balance calculation by *Elsig et al.* [2009] adding uncertainties to their net-fluxes. Changes in SST over the Holocene might have somewhat influenced pCO_2 and its $\delta^{13}C$ signature [*Joos et al.*, 2004; *Brovkin et al.*, 2008]. Circulation and marine productivity changes during the Holocene are generally thought to be relatively minor, except during the 8.2 ka event. However, no discernible imprint on atmospheric CO_2 [*Indermühle et al.*, 1999] is recorded for this rapid and well documented climate variation. A wild card is by how much the large reorganizations in ocean circulation and in the marine carbon cycle during the glacial/interglacial transition (18 to 11 ka B.P.) influenced the pCO_2 and $\delta^{13}CO_2$ evolution over the Holocene.

[9] This leads us to a number of guiding questions. Can we mechanistically explain the ocean air-sea fluxes that contributed to the atmospheric CO_2 and $\delta^{13}CO_2$ evolution? Are the mass balance estimates of *Elsig et al.* [2009] compatible with results from more mechanistic, process-oriented ocean models? Can the magnitude of land carbon stock changes be further constrained given a range of plausible deglacial-Holocene climate-carbon cycle evolutions? Can reconstructed changes in $\delta^{13}C$ of atmospheric CO_2 and of deep ocean DIC be quantitatively and concomitantly simulated?

2. Model and Experimental Setup

2.1. Bern3D+C Ocean Carbon Cycle Model

[10] The model used in this study is the Bern3D+C ocean carbon cycle model, which comprises an atmospheric, a terrestrial, an oceanic and a sedimentary reservoir. The physical ocean model, with a horizontal resolution of 36 × 36 grid boxes and 32 unevenly spaced layers, is a three-dimensional frictional geostrophic balance ocean model [*Müller et al.*, 2006], which has been further developed from the three-dimensional rigid-lid ocean model of *Edwards et al.* [1998] as updated by *Edwards and Marsh* [2005]. The atmospheric model is an Energy Balance Model (EBM), which details are described by *Ritz et al.* [2011]. The single-layer energy balance includes a hydrological cycle and has the same temporal and horizontal resolutions as the ocean model. The time-varying incoming insolation is calculated as a function of latitude using the algorithm of *Berger* [1978]. The marine biogeochemical cycle model is a 3-dimensional global model of the oceanic carbon cycle, fully coupled to the physical ocean model [*Parekh et al.*, 2008; *Tschumi et al.*, 2008]. The prognostic state variables considered in the model are dissolved inorganic carbon (DIC),

Table 1. Setup of Factorial Simulations Performed in This Study[a]

Simulation	Prescribed Forcing (Scenario Acronym)
	Shallow Water Carbonate Deposition
SWC1	Prescribed deposition of 0.315×10^{17} molC [after *Vecsei and Berger*, 2004] (VEC)
SWC2	Deposition following *Vecsei and Berger* [2004] during 18–8 ka B.P., constant deposition of 0.144 GtC/yr during 8–0 ka B.P. (R1, 1.04×10^{17} molC)
	Land Carbon Inventory Changes
LU1	404 GtC (404 + 0 + 0) uptake during the termination after *Menviel et al.* [2011] (LOV)
LU2	254 GtC (0 + 290-36) uptake during the Holocene after *Elsig et al.* [2009] (ELS)
LU3	658 GtC (404 + 290-36) uptake during the past 18 kyr (LOV-ELS)
	Radiative Forcing
DG1	Orbital, greenhouse gases and ice albedo forcing (DEGL)
DG2	As DG1, but with fixed SST in the biogeochemical model
DG3	As DG1, but without sediment module
DG4	As DG1, but with fixed SST in the biogeochemical model and without sediment module

[a]The labels VEC, LOV, ELS, and DEGL denote forcing scenarios from the literature. The numbers in parentheses indicate the land carbon inventory changes in GtC during three periods: the termination (18 to 11 ka B.P.), the early Holocene (11 to 5 ka B.P.), and the late Holocene (5 ka B.P. to preindustrial). The preindustrial, climatological sea surface temperatures are prescribed to compute the CO_2 solubility in simulations DG2 and DG4.

total alkalinity, ^{13}C, ^{14}C, phosphates (PO_4^{3-}), organic products, oxygen, silica and iron. New production is a function of temperature, light, phosphate and iron following *Doney et al.* [1996]. The competition between opal and calcite producers is modeled following the formulations of the HAMOCC5 model of *Maier-Reimer et al.* [2005]. ^{13}C fractionation occurs during marine photosynthesis [*Freeman and Hayes*, 1992] and the formation of calcium carbonate [*Mook*, 1988]. The air-sea gas exchange is implemented following OCMIP-2 [*Orr and Najjar*, 1999; *Najjar et al.*, 1999], but applying a linear relationship between wind speed and gas exchange rate [*Krakauer et al.*, 2006]. Air-sea ^{13}C exchange is subjected to kinetic fractionation [*Siegenthaler and Muennich*, 1981]. ^{14}C is represented as a fractionation-corrected concentration. The sedimentary component represents sediment formation, redissolution, remineralization as well as sediment diagenesis in the top 10 cm beneath the seafloor in the pelagic ocean [*Heinze et al.*, 1999; *Gehlen et al.*, 2006]. The accumulation of opal, $CaCO_3$ and organic matter is calculated on the basis of a set of dynamical equations for the sediment diagenesis process [*Tschumi et al.*, 2011]. The land carbon is represented by the 4-boxes model of *Siegenthaler and Oeschger* [1987].

2.1.1. Model Performances and Spin-Up

[11] Model performance with respect to individual model components is to some extent described in the literature. *Tschumi et al.* [2011] discuss the pre-industrial performance of the ocean-sediment components. The coupling of the ocean-sediment modules to the EBM leads to slight changes in ocean circulation and tracer distribution. A description of the initialization of the model and of the pre-industrial performances with the EBM can be found by *Ritz et al.* [2011]. The modeled temperature, salinity and phosphate distributions obtained in our pre-industrial run are similar to the ones shown by *Ritz et al.* [2011] and are thus in reasonable agreement with observations. Under pre-industrial conditions, the simulated export fluxes amount to 13.5 GtC/yr for organic matter, 1.2 GtC for $CaCO_3$ and 107 Tmol Si/yr for opal, in agreement with other modeling studies [*Jin et al.*, 2006].

[12] A model state for the LGM was obtained by forcing the model transiently with the time-varying changes in insolation [*Berger*, 1978], ice sheet extent as well as radiative changes due to the varying atmospheric CO_2 [*Lüthi et al.*, 2008] and CH_4 content [*Loulergue et al.*, 2008] starting from the last interglacial (125 ka B.P.) [*Ritz et al.*, 2011]. The ice sheet extent forcing uses the LGM ice sheet mask from *Peltier* [1994], which is scaled over the glacial inception on the global ice volume (benthic $\delta^{18}O$ stack [*Lisiecki and Raymo*, 2005]). The LGM SST field, $\delta^{13}C$ averaged over the Atlantic basin and deep [CO_3^{2-}] are shown in the auxiliary material as anomalies relative to the preindustrial state. The LGM $\delta^{13}C$ anomalies are compared to the paleo data compiled by []. Sensitivity simulations (not shown) strongly suggest that the modeled LGM biogeochemical state does not have a strong impact on the results presented for the Holocene.

2.2. Experiments Performed

[13] A number of factorial experiments were performed to disentangle the influence of individual mechanisms on atmospheric CO_2, $\delta^{13}C$ of CO_2 and DIC, and deep ocean carbonate concentration as detailed in Table 1 and Figures 1, 2, and 3. We also run a range of experiments with combined forcings as summarized in Table 2 and in the auxiliary material.[1]

2.2.1. Shallow-Water Carbonate Deposition, SWC

[14] Shallow-water carbonate deposition is not modeled explicitly but prescribed as an external flux as coastal areas are not resolved in our coarse resolution model. To mimic shallow-water carbonate deposition, alkalinity and DIC are uniformly removed from the surface ocean in a 2:1 ratio and at a rate consistent with the prescribed deposition scenario (Table 1). These experiments start from the pre-industrial state.

[15] *Vecsei and Berger* [2004] (Figure 1, black line) suggest a total shallow-water carbonate deposition on coral reefs, on isolated banks, and on continent attached platforms of 378 GtC (0.315×10^{17} molC) over the last 14 kyr. *Vecsei and Berger* [2004] label their total production as well as the doubling of production at 8 ka B.P. as conservative estimates. Indeed, production by shallow submerged reef is not taken into account. As the scenario suggested by *Vecsei and Berger* [2004] is much smaller than previous estimates [*Milliman*, 1993; *Kleypas*, 1997; *Ryan et al.*, 2001] and as *Vecsei and Berger*'s [2004] scenario might underestimate the shallow-water carbonate deposition for the last 8 kyr, another scenario (R1) is designed (Figure 1, red line), in which the total shallow-water carbonate deposition amounts to 1244 GtC (1.04×10^{17} molC) over the last 14 kyr. This corresponds to an average $CaCO_3$ deposition of 12 TmolC/yr over the last 8000 years, in agreement with the

[1]Auxiliary materials are available in the HTML. doi:10.1029/2011PA002224.

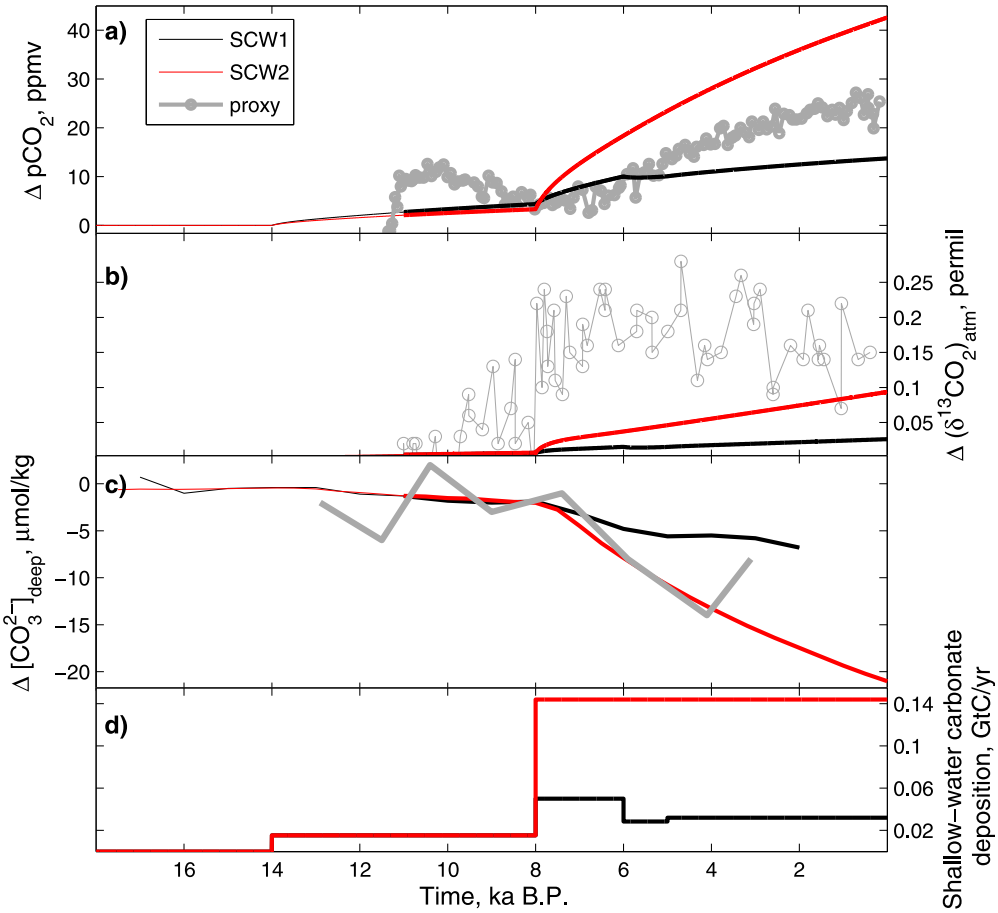

Figure 1. Response to changes in shallow-water carbonate deposition. Time series of anomalies in (a) atmospheric CO_2 (ppmv), (b) atmospheric $\delta^{13}CO_2$ (permil), (c) deep $[CO_3^{2-}]$ in the Caribbean Sea (μmol/kg) and (d) scenarios for coral reef growth (bottom, GtC/yr) used for experiment SCW1 (black) and SCW2 (red). The grey line represents atmospheric CO_2 anomalies (ppmv) (Figure 1a) as recorded in EPICA Dome C ice core [*Monnin et al.*, 2001], atmospheric $\delta^{13}CO_2$ anomalies (permil) (Figure 1b) as recorded in EPICA Dome C ice core [*Elsig et al.*, 2009] and deep $[CO_3^{2-}]$ anomalies (μmol/kg) (Figure 1c) in the Caribbean Sea as deduced from B/Ca data [*Yu et al.*, 2010b].

estimate by *Opdyke* [2000] and the model forcing applied by *Ridgwell et al.* [2003], but lower than the forcing applied by *Kleinen et al.* [2010]. Overall, there is substantial uncertainties in the magnitude and timing of shallow-water carbonate deposition with the estimates of *Vecsei and Berger* [2004] likely providing a lower limit and scenario R1 providing a high estimate.

2.2.2. Land Carbon Uptake and Release Scenarios, LU

[16] Our setup of the Bern3D+C does not include a comprehensive terrestrial carbon cycle model as the focus here is on marine processes. In the control set up, fluxes across the different land reservoirs and the atmosphere are set constant. To simulate changes in the terrestrial carbon, we therefore modify these fluxes following a given scenario of terrestrial carbon change.

[17] A range of data-based and model studies estimate the magnitude or the evolution of terrestrial organic carbon inventories over the past 20 kyr [e.g., *Curry et al.*, 1988; *Duplessy et al.*, 1988; *Bird et al.*, 1994; *Francois et al.*, 1998; *Beerling*, 1999; *Kaplan et al.*, 2002; *Joos et al.*, 2004; *Elsig et al.*, 2009; *Menviel et al.*, 2011]. Most estimates suggest an increase in land carbon in the range of 300 to 700 GtC over the last 18 kyr, compatible with the increase in deep ocean $\delta^{13}C$ of DIC of about 0.3 permil. Some authors however argue that terrestrial carbon storage was larger at the Last Glacial Maximum (LGM) than during the more recent preindustrial period [*Zeng*, 2003; *Zimov et al.*, 2009], a trend that is apparently in conflict with the reconstructed whole ocean $\delta^{13}C$ signal.

[18] *Menviel et al.* [2011] performed a transient simulation of the last deglaciation, including millennial-scale events such as Heinrich event 1 (H1), the Bølling-Allerød, the Antarctic Cold Reversal (ACR) and the Younger Dryas (YD) with the Earth System Model of Intermediate Complexity LOVECLIM. The changes in terrestrial carbon as simulated with LOVECLIM are linearly reduced over the period 18 to 11 ka by 230 GtC to account for carbon losses associated with the flooding of exposed and vegetated shelves during the deglacial sea level rise [*Joos et al.*, 2004; *Montenegro et al.*, 2006]. This scenario for the land carbon release during the termination (LOV) displays a glacial/interglacial terrestrial carbon change of 404 GtC. In this study, the LOV scenario serves as a reference for

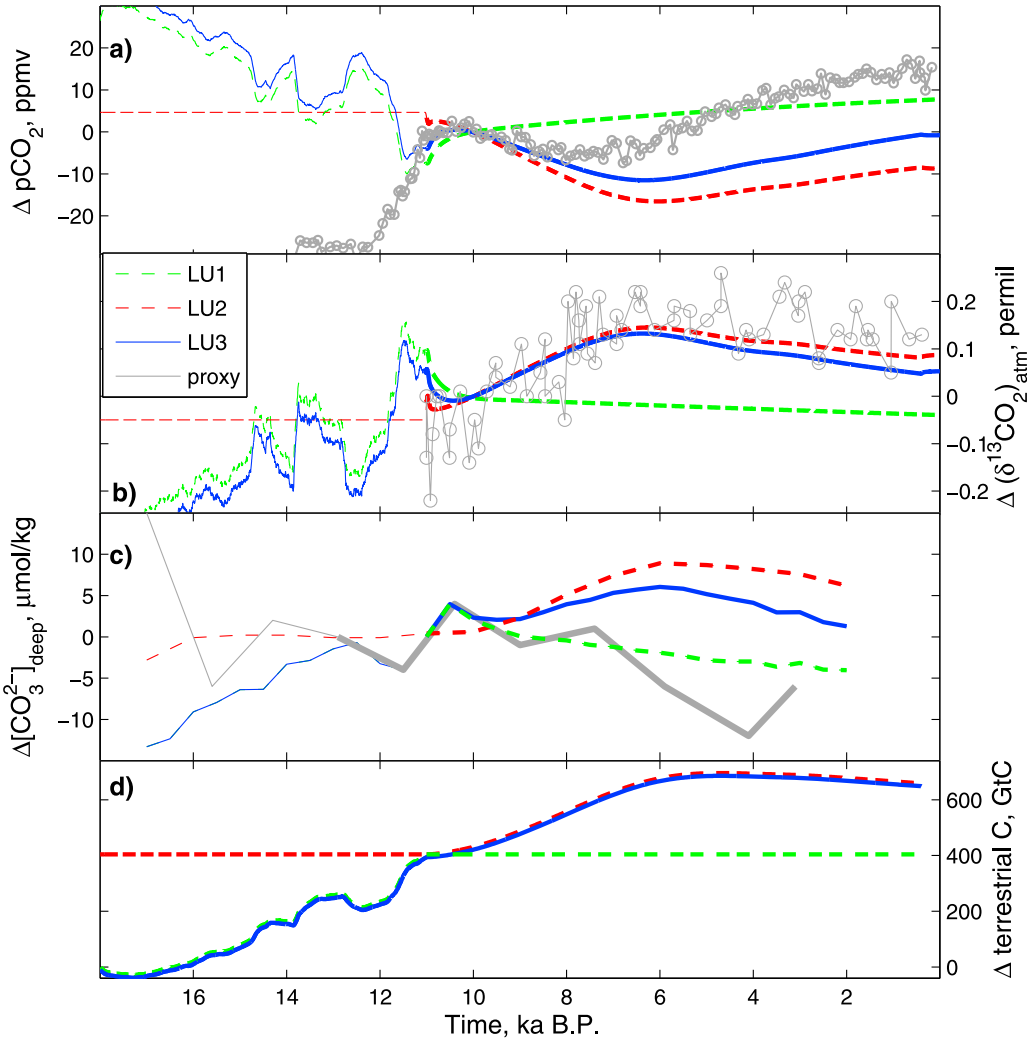

Figure 2. Response to changes in land carbon stocks. Time series of anomalies in (a) atmospheric CO_2 (ppmv), (b) atmospheric $\delta^{13}CO_2$ (permil), (c) deep $[CO_3^{2-}]$ in the Caribbean Sea (μmol/kg) for experiments LU1 (dashed green), LU2 (dashed red) and LU3 (blue). (d) Prescribed land carbon changes (GtC/yr). The grey line represents atmospheric CO_2 anomalies (ppmv) (Figure 2a) as recorded in EPICA Dome C ice core [*Monnin et al.*, 2001], atmospheric $\delta^{13}CO_2$ anomalies (permil) (Figure 2b) as recorded in EPICA Dome C ice core [*Elsig et al.*, 2009] and deep $[CO_3^{2-}]$ anomalies (μmol/kg) (Figure 2c) in the Caribbean Sea as deduced from B/Ca data [*Yu et al.*, 2010b].

terrestrial carbon changes during the last glacial termination (18–11 ka B.P.).

[19] Using a mass balance inverse calculation from EPICA Dome C atmospheric CO_2 and $\delta^{13}CO_2$ records, *Elsig et al.* [2009] estimate a terrestrial carbon uptake of 290 $\pm$ 36 GtC during the period 11–5 ka B.P. and a release of 36 $\pm$ 37 GtC thereafter (5 ka B.P. to 1560 AD). The uncertainties represent one standard deviation from a Monte Carlo analysis considering uncertainties in the input data only. Here, this reconstruction is used as our Holocene scenario (ELS) to force the Bern3D and to test its agreement with marine proxy data. In simulation LU1, LU2, and LU3, the land scenario LOV and ELS are applied separately and in combination (Figure 2 and Table 1) starting from the pre-industrial state.

[20] An alternative scenario to LOV-ELS is designed to explore a broader range of possible land carbon developments in combination with other forcings. Model results from LOVECLIM are combined with estimates of peat carbon uptake. At the end of the Younger Dryas, LOVECLIM simulates a rapid increase in the land carbon inventory of 160 GtC, which is not supported by proxy data. In scenario LOV2 this rapid post-YD increase is suppressed. Thereby, we implicitly assume that vegetation regrowth after the cessation of this northern hemisphere cold period progressed not as rapidly as simulated by LOVECLIM. Recent studies highlighted the possible role of carbon uptake by northern peatlands during the Holocene [*Tarnocai et al.*, 2009; *Wang et al.*, 2009; *Yu et al.*, 2010; *Yu*, 2010], a process not explicitly considered in current model studies and in LOVECLIM. Here, a linear carbon uptake of 550 GtC over the last 12 kyr due to peatland growth is included in the LOV2-YU scenario as guided by the results of *Yu et al.* [2010]. As LOVECLIM simulates a carbon release of ~65 GtC over the last 8 ka, in agreement with previous

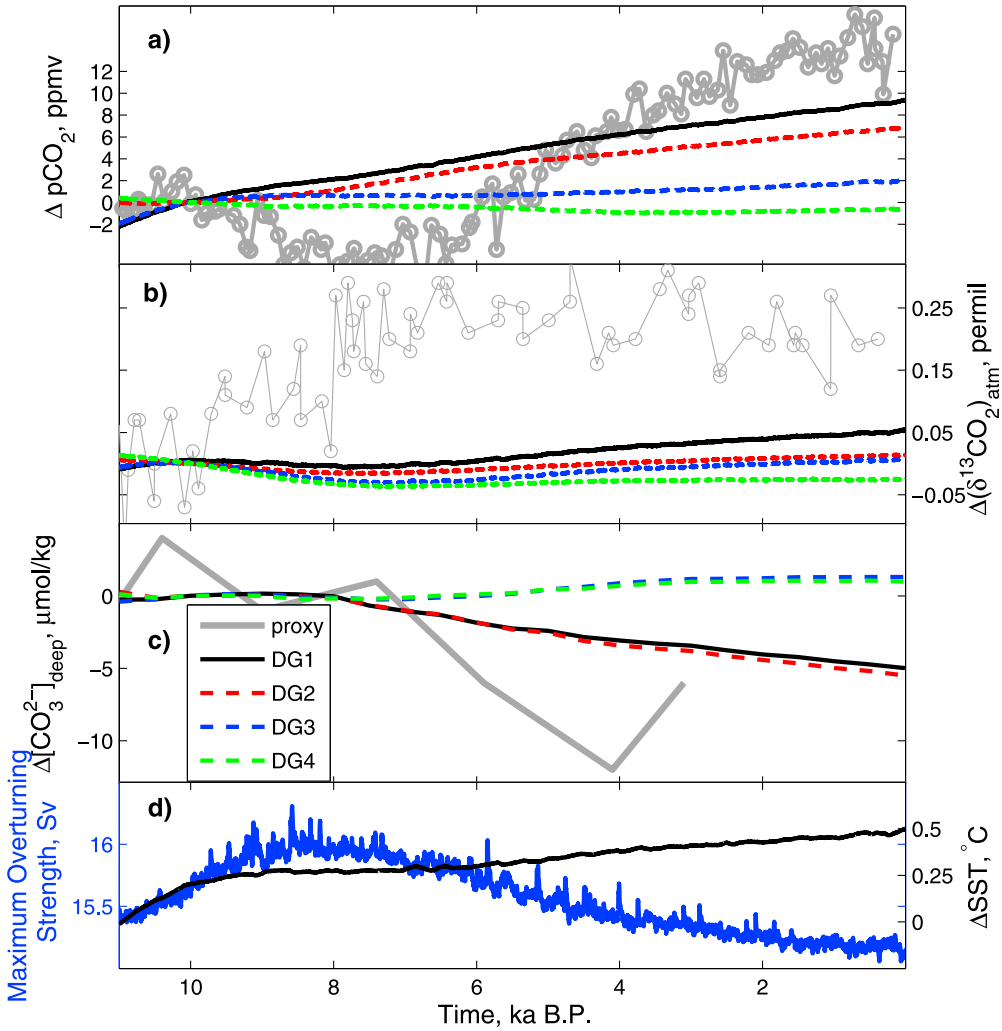

Figure 3. Response to changes in orbital, greenhouse gas, ice sheet and albedo forcing. Anomalies of (a) atmospheric CO_2 (ppmv), (b) atmospheric $\delta^{13}CO_2$ (permil) and (c) deep $[CO_3^{2-}]$ in the Caribbean Sea (μmol/kg) for experiments DG1 (black), DG2 (dashed red), DG3 (dashed blue), DG4 (dashed green). DG2 illustrates the variations induced by the carbonate compensation mechanism, DG3 represents the variations induced by changes in SST, circulation and other biogeochemical effects and DG4 illustrates the variations induced by circulation and other biogeochemical effects, while DG1 include all these mechanisms. The grey line represents atmospheric CO_2 anomalies (ppmv) (Figure 3a) and $\delta^{13}CO_2$ (Figure 3b) as recorded in EPICA Dome C ice core [*Monnin et al.*, 2001; *Elsig et al.*, 2009] and deep $[CO_3^{2-}]$ anomalies (μmol/kg) (Figure 3c) in the Caribbean Sea as deduced from B/Ca data [*Yu et al.*, 2010b]. (d) Time series of the maximum overturning stream function in the North Atlantic (Sv, blue) and the globally averaged SST anomalies (°C, black) for experiment DG1.

results [*Wang et al.*, 2005], the total land carbon uptake over the last 10 ka in scenario LOV2-YU amounts to 485 GtC. We consider this scenario as an illustrative upper limit case for Holocene carbon uptake and not as realistic. It neglects carbon release by anthropogenic land use [*Kaplan et al.*, 2010; *Stocker et al.*, 2011] and is in conflict with the mass balance estimate of *Elsig et al.* [2009].

[21] Finally, scenario LOV2-ELS2 is a slight modification of scenario LOV-ELS. Early Holocene land upake is increased from 290 to 325 GtC, consistent with the uncertainty band given by *Elsig et al.* [2009].

[22] The atmospheric CO_2 increase during the deglaciation can impact the land carbon uptake by stimulating photosynthesis [e.g., *Joos et al.*, 2004]. Scenarios LOV and LOV2-YU explicitly include this process called the CO_2 fertilization effect. The scenario ELS represents the sum of all the processes impacting land carbon changes during the Holocene and thus implicitly includes the CO_2 fertilization effect.

2.2.3. Radiative Forcing From Greenhouse Gases, Ice Albedo, and Orbital Variations, DG

[23] Simulations DG1 to DG4 are tailored to provide estimates of the influence on the Holocene carbon cycle of deglacial changes in SST, ocean circulation and related changes in the cycles of organic matter, calcite and ocean-

Table 2. Simulations Including a Combination of Forcings[a]

	Shallow Water Carbonate ($\times 10^{17}$molC)	Land Carbon (GtC)	Radiative Forcing
S1	VEC (0.315)	LOV-ELS (658 = 404 + 290-36)	DEGL
S2	VEC (0.315)	LOV2-YU (715 = 246 + 280 + 189)	DEGL
S3	R1 (1.04)	LOV-ELS (658 = 404 + 290-36)	DEGL
S4	R1 (1.04)	LOV2-YU (715 = 246 + 280 + 189)	DEGL
S5	VEC - 18–8 ka B.P. (0.375) VEC*1.1 - 8–6 ka B.P. VEC*2 - 6–3 ka B.P. VEC*1 - 3–2 ka B.P. VEC*0.5 - 2–0 ka B.P.	LOV2-ELS2 (535 = 246 + 325-36)	DEGL

[a]Literature references and further explanations of the acronyms for individual forcings are provided in Table 1. The shallow water carbonate deposition history of *Vecsei and Berger* [2004] (VEC) is modified in simulation S5 by scaling the original deposition rate by a constant factor during individual periods; total carbonate deposition in 10^{17} molC is given in parentheses. Land carbon inventory changes for the past 18 kyr, the termination (18 to 11 ka B.P.), the early Holocene (11 to 5 ka B.P.), and the late Holocene are given in GtC. LOV2 used in simulation S2, S4 and S5 is identical to the land carbon uptake scenario LOV [*Menviel et al.*, 2011] except that uptake is reduced between 12 and 11 ka B.P. ELS2 is a variant of the Holocene land carbon scenario ELS [*Elsig et al.*, 2009].

sediment interactions. The following experiments start from the LGM state.

[24] In simulation DG1, the model is transiently forced from the LGM to the pre-industrial state by prescribed changes in insolation [*Berger*, 1978], ice sheet extent [*Peltier*, 1994] as well as the radiative effect of atmospheric CO_2 [*Monnin et al.*, 2001] and atmospheric CH_4 content [*Loulergue et al.*, 2008]. Freshwater input in the ocean due to melting ice sheets is not taken into account in simulations DG1–DG4. The contributions of individual mechanisms to the changes simulated in DG1 are quantified by simulations DG2 to DG4 in which SST is kept at pre-industrial values in the biogeochemical part of the model (DG2 and DG4) and/or the sediment module is turned off (DG3 and DG4) (Table 1).

2.2.4. Freshwater Forcing Scenarios for the Representation of Abrupt Ocean Circulation Changes During the Last Termination

[25] The oceanic circulation most likely varied in response to freshwater input due to ice melting. As detailed in section 2 of Text S1, a number of freshwater experiments have been carried out to investigate the sensitivity of Holocene carbon cycle changes to deglacial circulation changes.

2.2.5. Model Simulations With All Forcings Included

[26] Simulations S1 to S5 are run with combined forcings as summarized in Table 2. Simulation S1 is forced by the original carbonate deposition history from *Vecsei and Berger* [2004] and the vegetation scenario LOV-ELS. To explore the impact on atmospheric CO_2 and $\delta^{13}CO_2$ of a different land carbon scenario, simulations S2 and S4 are forced with the LOV2-YU scenario. As the shallow-water carbonate deposition scenario suggested by *Vecsei and Berger* [2004] most likely represents a lower bound estimate, simulations S3 and S4 are forced with the upper bound estimate scenario R1. Finally, to get a close match with observations, we force simulations S5 with slightly modified land carbon uptake (LOV2-ELS2) and shallow-water carbonate deposition (VEC) scenarios.

3. Results From Factorial Simulations

3.1. Shallow-Water Carbonate Deposition

[27] We start discussion with results from the two factorial simulations in which only the shallow-water carbonate deposition is varied (Table 1 and Figure 1). Simulated changes in atmospheric CO_2, $\delta^{13}CO_2$, and deep ocean $[CO_3^{2-}]$ scale close to linear when the shallow-water carbonate deposition history is varied in simulations SWC1 and SWC2.

[28] The original *Vecsei and Berger* [2004] scenario leads to an atmospheric CO_2 increase of 14 ppmv (Figure 1 and Tables 3 and 4). Compared to observations, the slope of the atmospheric CO_2 increase after 6 ka B.P. is much smaller. In addition, atmospheric CO_2 never decreases in contrast to the ice core record. In experiment SCW2, atmospheric CO_2 increases by 42 ppmv. The slope of the atmospheric CO_2 between 8 and 6 ka B.P. is much larger than the one recorded in EPICA ice core. The pCO_2 increase per unit carbonate deposited is equivalent to the one obtained by *Ridgwell et al.* [2003] but is about 30% higher than the one reported by *Kleinen et al.* [2010], likely due to their use of a 2-dimensional ocean model.

[29] The impact on atmospheric $\delta^{13}CO_2$ of shallow-water carbonate deposition is relatively small but not negligible, especially for the high shallow-water carbonate deposition scenario (R1) (Figure 1b). In experiments SCW1 and SCW2, $\delta^{13}CO_2$ increases by respectively 0.02 permil and 0.09 permil. *Freeman and Hayes* [1992] showed that as atmospheric pCO_2 rises, the fractionation factor of ^{13}C during marine photosynthesis increases and thus the $\delta^{13}C$ of the organic matter produced decreases. Therefore, through a greater atmospheric CO_2, the deposition of shallow-water carbonate leads to a decrease in the $\delta^{13}C$ signature of marine organic matter and therefore to an increase in $\delta^{13}CO_2$. In addition, the stock of organic matter in the sediments increases leading to a higher signature of $\delta^{13}C_{DIC}$ and thus to an increase in $\delta^{13}CO_2$. In SCW1 and SCW2, the $\delta^{13}CO_2$ trend is positive from 6 to 0 ka B.P., at odds with reconstructions. In addition, shallow-water carbonate deposition cannot explain the strong ($\sim$0.15 permil) $\delta^{13}CO_2$ increase at 8 ka B.P.

[30] The deep $[CO_3^{2-}]$ in the Caribbean Sea decreases by 5 μmol/kg in SCW1 and by 21 μmol/kg in SCW2. The slope of the deep $[CO_3^{2-}]$ decrease between 7 and 4 ka B.P. in SCW2 is in close agreement with the reconstructed $[CO_3^{2-}]$ from B/Ca data [*Yu et al.*, 2010b] (Figure 1c). However, the youngest B/Ca data is at 3 ka B.P. and at a value much higher than the one reconstructed for 4 ka B.P. It is thus not

Table 3. Summary of Results Illustrating the Different Contributions to Changes in Atmospheric CO_2, $\delta^{13}CO_2$ and Deep CO_3^{2-} Concentrations Over the Period 10–7 ka B.P.[a]

Changes From 10 to 7 ka B.P.	Δ pCO_2 (ppmv)	Δ $\delta^{13}CO_2$ (permil)	Δ $[CO_3^{2-}]$ (μmol/kg)
Simulated Changes Compared to Proxy-Based Reconstructions			
Simulation S1	−3.1	+0.12	−1
Simulation S5	−5	+0.14	−1
Reconstructions	−5	+0.19	−1.5
Attribution to Individual Processes			
Shallow-water carbonate deposition (SCW1/VEC)	+3.8	+0.008	−1.6
Land uptake during termination (LU1/LOV)	+3.3	−0.02	−5.2
Land uptake during Holocene (LU2/ELS)	−14.8	+0.14	+7.1
Sediment interactions related to radiative forcing (DG2-DG4)	+2.5	+0.02	−0.9
Changes in CO_2 solubility (DG1-DG2)	+1	+0.01	0
Changes in circulation and export production without sediment interactions (DG4)	−0.3	−0.036	−0.1
$\sum$	−4.5	+0.12	−0.7

[a]The attribution to mechanisms is for simulation S1 and based on published forcing scenarios. The estimates for atmospheric CO_2, $\delta^{13}CO_2$ and deep $[CO_3^{2-}]$ are from *Monnin et al.* [2001], *Elsig et al.* [2009] and *Yu et al.* [2010b].

possible to know the deep $[CO_3^{2-}]$ trend in the Caribbean Sea between 4 and 0 ka B.P.

[31] In brief, coral reef growth and other shallow-water carbonate deposition during the last glacial termination and the Holocene probably contributed significantly to the Holocene evolution of atmospheric CO_2 and deep ocean $[CO_3^{2-}]$, but cannot explain the reconstructed $\delta^{13}CO_2$ variations nor the early Holocene pCO_2 decrease.

3.2. Land Carbon Uptake and Release

[32] Next, we discuss the factorial simulations where land carbon inventories are changed either during the glacial termination or the Holocene or during both periods (Figure 2). A substantial land carbon uptake over the transition of 400 GtC as applied in simulation LU1 causes an almost linear increase in pCO_2 of 8 ppmv over the Holocene in response to carbonate compensation, a strong decrease in $\delta^{13}CO_2$ between 11 and 10 ka and a slight decrease thereafter. Deep ocean $[CO_3^{2-}]$ decreases over the Holocene by about 5 μmol/kg.

[33] Simulations that include the Holocene uptake and release scenario from *Elsig et al.* [2009] (simulations LU2, LU3) match the reconstructed Holocene $\delta^{13}CO_2$ variations. In contrast, the simulated pCO_2 decrease in the early Holocene is larger than reconstructed.

[34] Deep ocean $[CO_3^{2-}]$ increases during the period of land uptake and decreases thereafter due to ongoing carbonate compensation. For the combined scenario of *Menviel et al.* [2011] and *Elsig et al.* [2009] (LOV-ELS, simulation LU3), $[CO_3^{2-}]$ in the deep Caribbean Sea increases by 18 μmol/kg over the transition and the early Holocene when land carbon is prescribed to increase by 694 GtC. The recovery from this perturbation is slow as indicated by the slight negative trend in $[CO_3^{2-}]$ after 6 ka B.P. (Figure 2c).

[35] Another interesting metric is the change in the average oceanic $\delta^{13}C_{DIC}$. On millennial timescales, these changes are indicative of the amount of organic carbon that is transferred to inorganic carbon or vice versa. Generally, changes in the average $\delta^{13}C_{DIC}$ are interpreted as a change in the carbon storage on land by assuming that the organic matter pool in the ocean remained unchanged [*Shackleton*, 1977; *Bird et al.*, 1994]. In the factorial experiments with land carbon changes only, the perturbation in the atmosphere and ocean go in parallel. The total oceanic $\delta^{13}C_{DIC}$ increases

Table 4. Same as Table 3 but for the Period 7–0 ka B.P.

Changes From 7 to 0 ka B.P.	Δ pCO_2 (ppmv)	Δ $\delta^{13}CO_2$ (permil)	Δ $[CO_3^{2-}]$ (μmol/kg)
Simulated Changes Compared to Proxy-Based Reconstructions			
Simulation S1	+19.6	−0.01	−16
Simulation S5	+19.4	0	−16
Reconstructions	+20	−0.04	−10
Attribution to Individual Processes			
Shallow-water carbonate deposition (SCW1/VEC)	+4.8	+0.014	−3.6
Land uptake during termination (LU1/LOV)	+5	−0.02	−4.3
Land uptake during Holocene (LU2/ELS)	+5.3	−0.04	−0.7
Sediment interactions related to radiative forcing (DG2-DG4)	+5	+0.017	−5.6
Changes in CO_2 solubility (DG1-DG2)	+1.6	+0.026	+0.5
Changes in circulation and export production without sediment interactions (DG4)	−0.4	+0.01	+1.1
$\sum$	+21.3	+0.007	−12.6

by 0.35 permil over the past 18 ka in simulation LU3 forced with the combined LOV-ELS scenario. For comparison, data-based estimates of whole ocean $\delta^{13}C_{DIC}$ changes are of about 0.3 permil [*Duplessy et al.*, 1988; *Curry et al.*, 1988]. A total carbon uptake since the LGM of 658 GtC, as prescribed in the LOV-ELS scenario (simulation LU3), is compatible with the proxy-based $\delta^{13}C_{DIC}$ change, but may correspond to an upper bound.

[36] In conclusion, land uptake over the termination contributes to the evolution of Holocene pCO_2 and deep ocean $[CO_3^{2-}]$ through the carbonate compensation mechanism, but its potential to affect atmospheric $\delta^{13}C$ is largely restricted to the termination and the first one or two millennia thereafter. On the other hand, the carbon fluxes reconstructed by *Elsig et al.* [2009] with their simplified mass balance/box model approach appear to explain most of the atmospheric $\delta^{13}C$ variations over the last 9 kyr also in the Bern3D model. As already highlighted by these authors, additional processes such as shallow-water carbonate deposition are required to close the Holocene pCO_2 budget.

3.3. Radiative Forcing From Greenhouse Gases, Ice Albedo, and Orbital Variations

[37] In this section, we discuss results from simulations DG1 to DG4 (Figure 3) in which radiative forcing from CO_2, CH_4, ice albedo, and orbital parameters are varied over the termination and the Holocene (Table 1). These simulations allow us to quantify the total changes induced by these forcings as well as to attribute the simulated changes to specific mechanisms.

[38] Due to the greater radiative forcing, the simulated globally averaged SST increases by 2.6°C over the last 18 kyr and by 0.25°C over the past 10 kyr (Figure 3). In addition, the strength of the AMOC increases from 11.5 Sv (18 ka B.P.) to peak at 16 Sv in the early Holocene and to decrease by about 1 Sv thereafter. The changes in the physical climate system undoubtedly affect the carbon cycle in the Holocene. Simulated atmospheric CO_2 increases by 9.4 ppmv between 10 and 0 ka B.P. and with an approximately constant rate of 1 ppmv per kyr (simulation DG1, Figure 3). About a quarter of this increase is due to a decrease in the solubility of CO_2 related to the Holocene SST increase (2.6 ppmv, DG1–DG2). Three quarter of the CO_2 increase are related to the long-term response of marine sediments to the changes simulated over the glacial termination (7.5 ppmv, DG2–DG4). This long-term sediment adjustment is due to variations in the ocean-sediment fluxes of CaCO3, organic matter, and opal during the transition. On the other hand, Holocene changes in circulation and export productivity have a small influence on pCO_2 (-0.7 ppmv, DG4). Simulated marine export production increases by 9% until 10 ka B.P., but changes only slightly (-1%) during the last 10 kyr.

[39] Atmospheric $\delta^{13}CO_2$ increases by about 0.05 permil during the last 7 kyr, mainly because of the global mean SST increase. Simulated $\delta^{13}CO_2$ changes are small over the early Holocene due to offsetting effects of the different contributing factors. Deep ocean $[CO_3^{2-}]$ increases by 25μmol/kg during the transition and decreases by about 5 μmol/kg during the Holocene, primarily due to ocean-sediment interactions.

[40] The modeled globally averaged SST increase of 0.2°C from 6 to 0 ka B.P. is in good agreement with an alkenone-based reconstruction compiled in the GHOST database [*Kim et al.*, 2004; *Kim and Schneider*, 2004] as well as with other modeling studies. Results from the PMIP2 experiments suggest a global SST increase of 0.2°C between 6 and 0 ka B.P. in the MIROC3.2 model and a 0.1°C increase in the NCAR CCSM model. In Bern3D+C, the reduced solubility due to the greater SST leads to an atmospheric CO_2 increase of about 2 ppmv for the past 6 kyr, comparable to an earlier study [*Joos et al.*, 2004]. This is in contrast to the suggestion of *Brovkin et al.* [2008] that a negative SST trend in the North Atlantic dominates the global signal and causes atmospheric CO_2 to decrease. These authors applied reconstructed SST changes from the GHOST database north of 30°S in the CLIMBER-2 and CLIMBER-3α model and obtained an atmospheric CO_2 decrease of 6 and 1 ppmv, respectively. However, CLIMBER-2 is a zonally averaged model, CLIMBER-3α was only run for 300 years, and the Southern Ocean was excluded from the study due to a lack of data.

[41] In conclusion, changes in greenhouse gases forcing, ice albedo and orbital parameters cause major changes in circulation, marine productivity and SST over the glacial termination. This, in turn, leads to a substantial increase in pCO_2 over the Holocene due to the long adjustment timescales of marine sediments as further evidenced by the declining trend in deep ocean $[CO_3^{2-}]$. Adding the impact of SST driven CO_2 outgassing yields a Holocene pCO_2 increase of 10 ppmv. This signal of the glacial termination has not yet been included in earlier model studies addressing Holocene pCO_2 variations.

4. Results From Model Simulations With Multiple Forcings

[42] As detailed in Table 2, we perform five experiments with all the forcings included, in which we test two shallow-water carbonate deposition (lower limit:VEC and upper limit: R1) and three land carbon changes scenarios (LOV-ELS and LOV2-YU and LOV2-ELS2).

4.1. Simulations With Scenarios From the Literature

[43] As seen in Figure 4 (blue line), a good match with the various proxy records is obtained when the Bern3D is forced with land carbon changes as suggested by *Menviel et al.* [2011] and *Elsig et al.* [2009] (LOV-ELS), shallow-water carbonate deposition as suggested by *Vecsei and Berger* [2004] (VEC) as well as deglacial changes in greenhouse gases, ice albedo, and orbital parameters. The main difference between the simulated atmospheric CO_2 in experiment S1 and the EPICA Dome C ice core record is the magnitude of the atmospheric CO_2 decrease between 10 and 7 ka B.P. While the atmospheric CO_2 measured in EPICA Dome C [*Monnin et al.*, 2001] decreases by about 7 ppmv, the atmospheric CO_2 simulated in experiment S1 decreases by only 4 ppmv. Tables 3 and 4 provide an attribution of the simulated changes in S1 to individual mechanisms for the early Holocene (10 to 7 ka B.P.) and the past 7 kyr, respectively.

[44] When the Bern3D is forced with the shallow-water carbonate deposition suggested by *Vecsei and Berger* [2004]

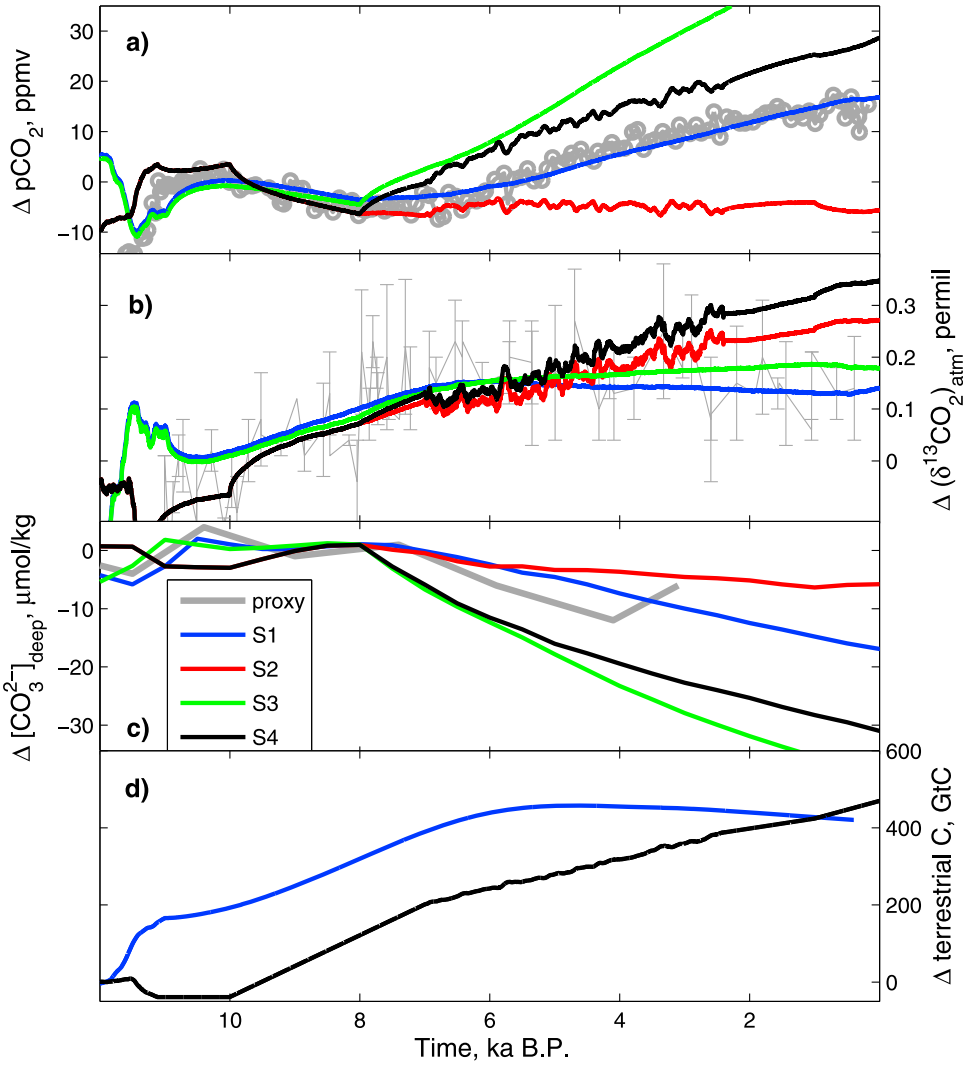

Figure 4. Responses to combinations of forcings. Anomalies of (a) atmospheric CO_2 (ppmv), (b) atmospheric $\delta^{13}CO_2$ (permil), (c) deep $[CO_3^{2-}]$ in the Caribbean Sea (μmol/kg) and (d) deep $\delta^{13}C_{DIC}$ for experiments S1 (blue), S2 (red), S3 (green) and S4 (black). The grey line represents atmospheric CO_2 anomalies (ppmv) (Figure 4a) and $\delta^{13}CO_2$ (Figure 4b) as recorded in EPICA Dome C ice core [*Monnin et al.*, 2001; *Elsig et al.*, 2009], deep $[CO_3^{2-}]$ anomalies (μmol/kg) (Figure 4c) in the Caribbean Sea as deduced from B/Ca data [*Yu et al.*, 2010b]. Time series of the land carbon changes applied: LOV-ELS (blue) and LOV2-YU (black) (Figure 4d).

(VEC) and a land carbon change that takes into account peat buildup during the Holocene as suggested by *Yu et al.* [2010] (LOV2-YU, simulation S2, red line in Figure 4), then the simulated atmospheric CO_2 only increases by 1 ppmv during the last 8 kyr. In addition, the slope of the atmospheric $\delta^{13}CO_2$ increase in the last 7 kyr is much greater than the one recorded in EPICA Dome C ice core.

[45] Simulation S3 (green line in Figure 4), forced with the high shallow-water carbonate deposition scenario (R1) and the LOV-ELS terrestrial carbon scenario, leads to a 55 ppmv pCO_2 increase over the last 8 kyr, which clearly overestimate the observed 20 ppmv late Holocene increase. In addition, the strong deposition of shallow-water carbonate applied leads to a 38 μmol/kg decrease in deep $[CO_3^{2-}]$ in the Cariaco basin in disagreement with the deep $[CO_3^{2-}]$ inferred from B/Ca data [*Yu et al.*, 2010b]. On the other hand, as the $\delta^{13}CO_2$ is mainly influenced by changes in terrestrial carbon, the simulated $\delta^{13}CO_2$ in S3 is in good agreement with observations.

[46] Experiment S4, forced with the high shallow-water carbonate deposition scenario (R1) and the terrestrial carbon scenario including Holocene peat build up (LOV2-YU) overestimates the atmospheric CO_2 increase and the $\delta^{13}CO_2$ increase of the last 7 kyr by 13 ppmv and 0.2 permil respectively. If we perform an additional experiment (not shown) forced with the terrestrial carbon scenario LOV2-YU and a shallow-water carbonate deposition scenario as suggested by *Vecsei and Berger* [2004] until 8 ka B.P. followed by a constant deposition of 0.11 GtC/yr, then we can reconcile the simulated atmospheric CO_2 with the EPICA

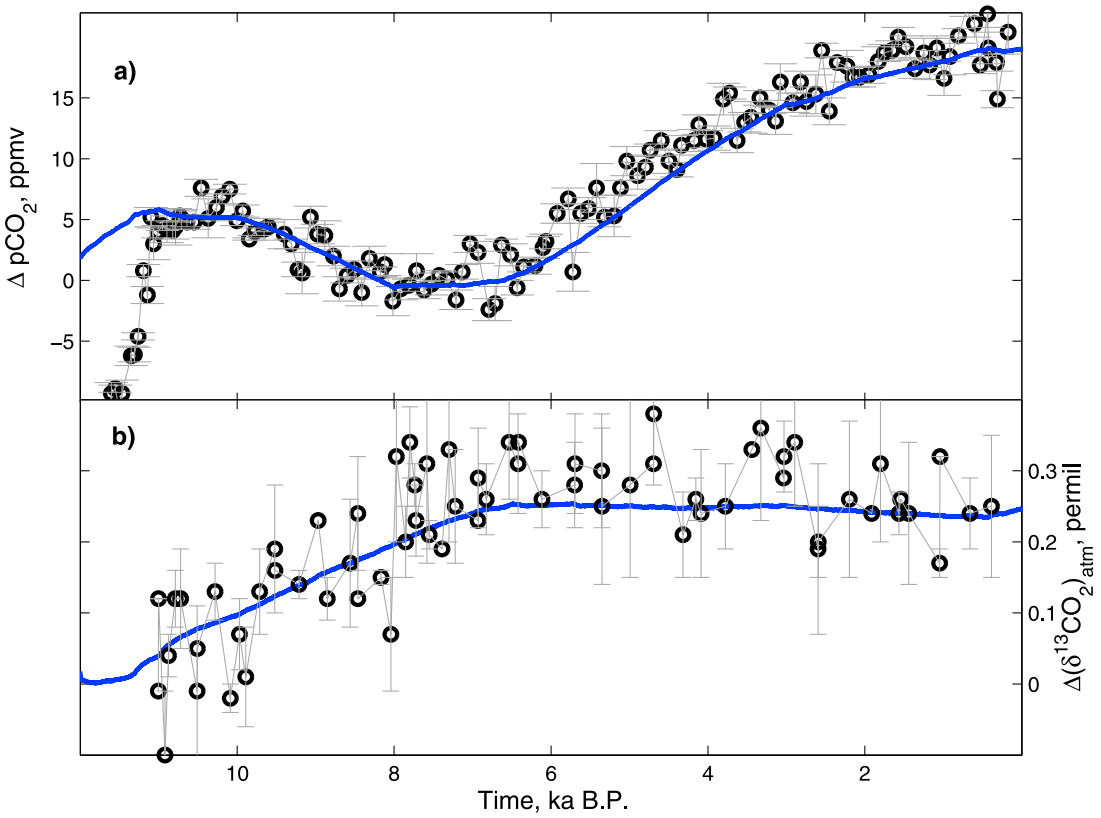

Figure 5. (a) Atmospheric CO_2 and (b) $\delta^{13}CO_2$ anomalies as simulated in experiment S5 compared to the EPICA Dome C ice core record [*Monnin et al.*, 2001; *Elsig et al.*, 2009].

Dome C ice core record. However, the slope of the simulated $\delta^{13}CO_2$ increase is similar to the one obtained in experiment S4. We perform a Monte Carlo analysis on the $\delta^{13}CO_2$ from EPICA Dome C ice core to estimate the mean and standard deviation of the linear trend over the last 7 ka. The probability density function obtained indicates a mean $\delta^{13}CO_2$ slope of 0.0012 permil/ka over the last 7 ka with a mean standard deviation of 0.0011 permil/ka. With a mean slope of 0.036 permil/ka, experiment S4 clearly falls outside of the 2 standard deviation confidence interval. Even by taking into account the uncertainties associated with the EPICA Dome C ice core reconstructions, we cannot reconcile scenario S4 with observations.

[47] Simulations S1–S4 show that the Holocene atmospheric CO_2 variations result from a fine balance between shallow-water carbonate deposition and land carbon changes. The combination of the shallow-water carbonate deposition suggested by *Vecsei and Berger* [2004] and the changes in land-atmosphere carbon fluxes suggested by *Elsig et al.* [2009] lead to a good agreement with observations and can thus serve as a baseline. A greater shallow-water carbonate deposition than the one suggested by *Vecsei and Berger* [2004] has to be compensated by a greater land carbon uptake than the one inferred from the mass balance suggested by *Elsig et al.* [2009]. However, atmospheric $\delta^{13}CO_2$ is mainly influenced by terrestrial processes and gives another strong constraint on terrestrial carbon changes: a strong land carbon uptake will lead to an overestimation of the atmospheric $\delta^{13}CO_2$ changes during the Holocene.

4.2. Toward Explaining the Ice Core and Marine Proxy Records

[48] An even better agreement with the ice core data is achieved by slightly adjusting the land carbon (LOV-ELS) and carbonate deposition (VEC) scenarios in simulation S5. Then, the Bern3D model is able to simulate the reconstructed evolution in atmospheric CO_2 and $\delta^{13}CO_2$ during the entire Holocene within the uncertainties of the ice core data (Figure 5, blue line).

[49] The LOVECLIM results of *Menviel et al.* [2011] as applied in S1 suggest a 150 GtC land uptake between 11.8 and 11 ka B.P., implying a fast growth of the terrestrial vegetation after the YD. To account for a possible slower increase in the land carbon storage at the end of the YD, the land carbon uptake is almost suppressed between 11.8 and 11 ka B.P. in simulation S5. In turn, the uptake during the early Holocene is increased by 35 GtC. Shallow-water carbonate deposition is modified as detailed in Table 2. The total deposition is increased by ~25% over the last 8 kyr to promote a somewhat larger late Holocene pCO_2 increase in the model. The modifications are well within uncertainties of the literature-based estimates. We conclude that the Holocene variations in pCO_2 and $\delta^{13}CO_2$ are explained by the subtle combination of a range of processes including land carbon changes, shallow-water carbonate deposition, marine sediment adjustments to earlier land carbon changes and to changes in the marine carbon cycle over the glacial termination as well as SST changes driven by orbital variations, greenhouse gases and ice albedo forcing.

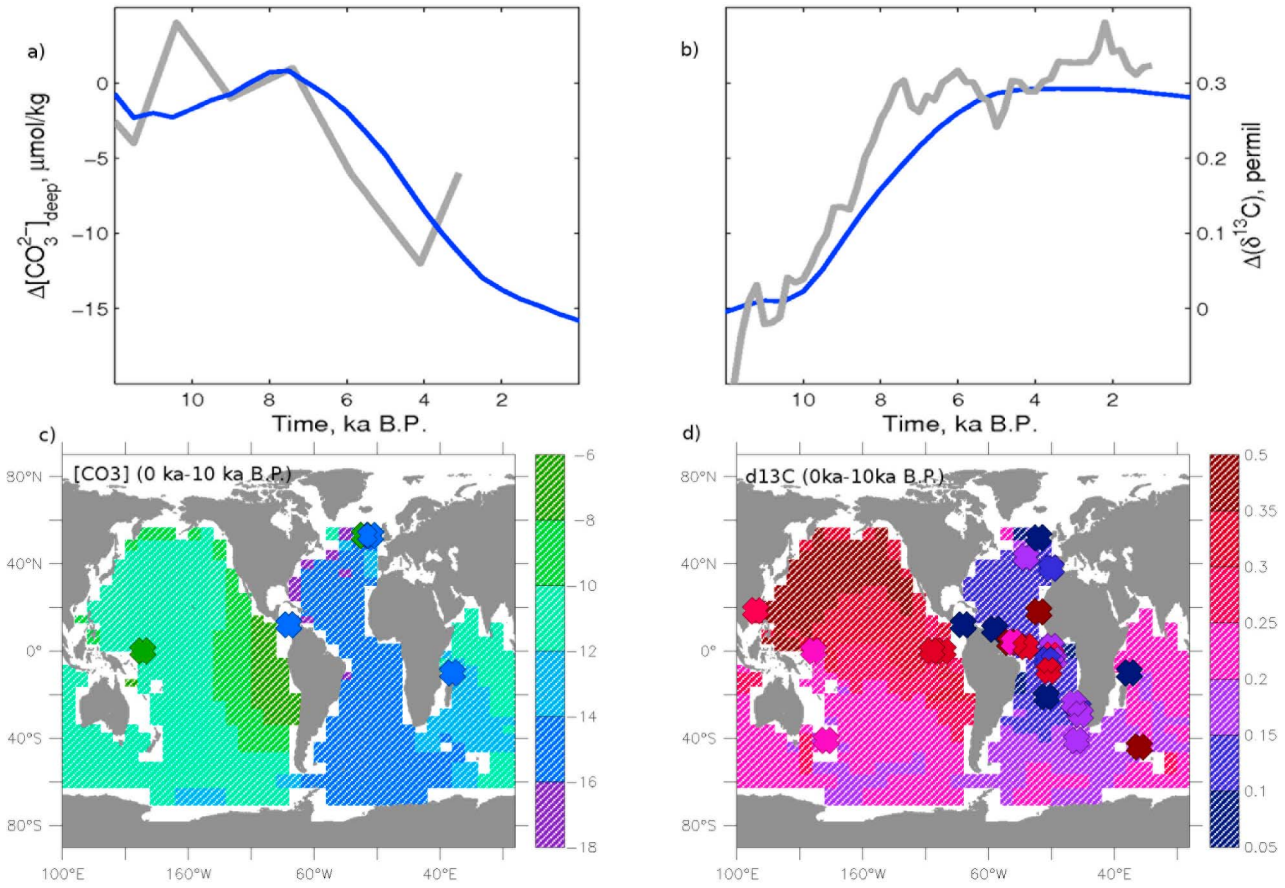

Figure 6. Simulated and proxy-based spatiotemporal evolution of deep ocean $[CO_3^{2-}]$ and $\delta^{13}C$ of DIC. (a) Time series of deep $[CO_3^{2-}]$ anomalies in the Caribbean Sea (μmol/kg) and (b) $\delta^{13}C$ anomalies (permil) as simulated in the deep ocean (≥3000 m) for experiments S5 (blue). The grey curve represents deep $[CO_3^{2-}]$ (Figure 6a) as deduced from B/Ca data [*Yu et al.*, 2010b] and a stack of benthic $\delta^{13}C$ data (Figure 6b) from marine sediment coresRC13-110 [*Mix et al.*, 1991], MD97-2121 [*Carter et al.*, 2008], CHAT10K [*McCave et al.*, 2008], SO50-31KL [*Wei et al.*, 2006], CHN82-24, KNR 73-3/4 [*Boyle and Keigwin*, 1985], V30-49 [*Mix and Fairbanks*, 1985], CH75-04, KNR 110-75, KNR 110-71, KNR 110-66 [*Curry et al.*, 1988], RC13-229 [*Oppo and Fairbanks*, 1987], MD84-527 [*Labeyrie et al.*, 1987], MW91-9 GGC48, BOFS 8K, WIND28K [*Yu et al.*, 2010a], GeoB-1034, GeoB-1041, GeoB-1101, GeoB-1105, GeoB-1112, GeoB-1115, GeoB-1118, GeoB-1211 [*Bickert and Wefer*, 1996], GeoB-1520, GeoB-1721, GeoB-4403, GeoB-5115 [*Bickert and Mackensen*, 2003], GeoB-1523 [*Mulitza*, 1998], GeoB-1903 [*Dürkop et al.*, 1997], GeoB-1214, GeoB-1710 [*Schmiedl and Mackensen*, 1997] and GeoB-1722 [*Mollenhauer et al.*, 2002]. (c) Deep (2300–4200 m) $[CO_3^{2-}]$ anomalies (μmol/kg) over the Holocene (0–10 ka B.P.) for experiment S5. Overlaid are $[CO_3^{2-}]$ anomaly estimates from marine sediment cores (from West to East) MW91-9 GGC15, MW91-9 GGC48, VM28-122, BOFS 8K and WIND28K [*Yu et al.*, 2010a]. (d) Deep (≥3000 m) $\delta^{13}C$ anomalies (permil) over the Holocene (0–10 ka B.P.) for experiment S5. Overlaid are $\delta^{13}C$ anomaly estimates from the same marine sediment cores used in the benthic $\delta^{13}C$ stack above plus ODP 1089 [*Hodell et al.*, 2003] and MD95-2042 [*Pailler and Bard*, 2002].

[50] Is the Bern3D model also able to represent the spatiotemporal evolution of deep ocean $\delta^{13}C_{DIC}$ and of $[CO_3^{2-}]$ as reconstructed from marine sediments? Simulation S5 represents relatively well the deep $[CO_3^{2-}]$ in the Caribbean Sea as suggested by the B/Ca of *Yu et al.* [2010b] (Figure 6a). Both proxy data and model indicate that most of the decrease in $[CO_3^{2-}]$ is realized after 7 ka B.P. in the deep Caribbean Sea. Similarly, reconstructed and simulated $\delta^{13}C_{DIC}$ in the deep ocean [*Boyle and Keigwin*, 1985; *Mix and Fairbanks*, 1985; *Labeyrie et al.*, 1987; *Oppo and Fairbanks*, 1987; *Curry et al.*, 1988; *Mix et al.*, 1991; *Bickert and Wefer*, 1996; *Dürkop et al.*, 1997; *Schmiedl and Mackensen*, 1997; *Mulitza*, 1998; *Mollenhauer et al.*, 2002; *Bickert and Mackensen*, 2003; *Wei et al.*, 2006; *Carter et al.*, 2008; *McCave et al.*, 2008; *Yu et al.*, 2010a] increased in the early Holocene and remained approximately constant after 6 ka B.P. (Figure 6b).

[51] The comparison with sediment cores shows that not only the simulated temporal tracer evolution is well represented in the model, but also the spatial pattern. Results from

simulation S5 suggest that deep ocean $[CO_3^{2-}]$ decreased by $\sim$15 μmol/kg in the Atlantic and by $\sim$10 μmol/kg in the Pacific from 10 ka B.P. to preindustrial. Deep ocean $\delta^{13}C_{DIC}$ is simulated to increase over the Holocene by about 0.15 permil in the deep North Atlantic, by 0.2 permil in the deep southern Pacific and Indian Ocean and by 0.4 permil in the deep North Pacific. Both patterns of change are in reasonable quantitative agreement with the available marine sediment proxy data (Figures 6c and 6d) [*Boyle and Keigwin*, 1985; *Mix and Fairbanks*, 1985; *Labeyrie et al.*, 1987; *Oppo and Fairbanks*, 1987; *Curry et al.*, 1988; *Mix et al.*, 1991; *Bickert and Wefer*, 1996; *Dürkop et al.*, 1997; *Schmiedl and Mackensen*, 1997; *Mulitza*, 1998; *Mollenhauer et al.*, 2002; *Bickert and Mackensen*, 2003; *Hodell et al.*, 2003; *Wei et al.*, 2006; *Martrat et al.*, 2007; *McCave et al.*, 2008; *Yu et al.*, 2010a]. The model yields large tracer gradients in the deep Southern Ocean which are likely related to the too weak circumpolar circulation of our coarse resolution model.

[52] Total carbon uptake since the LGM is prescribed to 535 GtC in S5. This yields an increase in the average $\delta^{13}C_{DIC}$ in the ocean of 0.4 permil, which is consistent with proxy-based estimates [*Duplessy et al.*, 1988; *Curry et al.*, 1988; *Bird et al.*, 1994].

[53] We conclude that the Bern3D results for S5 are not only in agreement with the Holocene ice core data, but also in agreement with the available marine sediment proxy information on Holocene $[CO_3^{2-}]$ and $\delta^{13}C_{DIC}$ changes in the deep ocean as well as with information on the change in the average $\delta^{13}C_{DIC}$. This provides further evidence that the multimechanism forcing scenario S5 gives a plausible and consistent explanation of the Holocene carbon cycle variations.

4.3. Alternative Scenarios

[54] The scarcity, the low resolution, and the high variability of marine sediment records for the Holocene make it difficult to draw firm conclusions with respect to the Holocene evolution of deep ocean $[CO_3^{2-}]$ and $\delta^{13}C_{DIC}$. This may suggest that other forcing scenarios could also yield a good representation of the ice core record and still be compatible with the marine proxy data. Notably, the land carbon uptake during the transition and early Holocene as well as the shallow-water-carbonate deposition have similar influences on atmospheric CO_2 and $\delta^{13}CO_2$ during the late Holocene. These processes tend to promote a late Holocene rise in pCO_2, while hardly affecting $\delta^{13}CO_2$ during the late Holocene. For example, a scenario with a terrestrial release (instead of an uptake) during the termination and shallow water carbonate deposition totaling about 30% more than in VEC is also consistent with the Holocene CO_2 and $\delta^{13}CO_2$ ice records (see Table 2 in Text S1 and Figure S5).

[55] In addition, the potential influence of rapid changes in ocean circulation during the transition has not been considered in simulations S1–S5. Results of experiments including changes in ocean circulation during the termination (18–11 ka B.P.) are shown in the auxiliary material. These results suggest that oceanic reorganizations during the Younger Dryas (YD) and the Antarctic Cold Reversal (ACR) could have a significant impact on atmospheric CO_2, $\delta^{13}CO_2$, and carbonate concentrations between 11 and 9 ka B.P., while they would have a small influence on the period after 9 ka B.P.

5. Discussion and Conclusions

[56] The Holocene ice core records of atmospheric CO_2 and $\delta^{13}CO_2$ are represented within their uncertainties, when forcing the Bern3D+C model with published estimates of land carbon changes, shallow-water carbonate deposition as well as greenhouse gases, ice albedo and orbital variations during the past 18 kyr (Figure 5). In addition, the model is able to reproduce the spatiotemporal evolution of $[CO_3^{2-}]$, deep ocean $\delta^{13}C_{DIC}$ (Figure 6) and the overall change in $\delta^{13}C_{DIC}$ from the LGM to the late Holocene.

[57] The decrease in atmospheric CO_2 in the early Holocene and the 20 ppmv increase during the last 7 kyr is the result of a subtle balance of a range of processes. The atmospheric CO_2 and $\delta^{13}CO_2$ changes observed during the Holocene can be explained by (1) the long term response of the ocean-sediment-atmosphere system to climate and marine changes during the termination, (2) shallow-water carbonate deposition, (3) carbonate compensation following a deglacial terrestrial carbon uptake, (4) net land carbon uptake between 11 and 5 ka B.P., and (5) a 0.25°C increase in global SST and related changes in CO_2 solubility.

[58] For the first time, the influence on Holocene pCO_2 of changes in greenhouse gases, ice albedo and orbital parameters occurring during the glacial termination (18–11 ka B.P.) was quantified with a spatially resolved mechanistic model. These forcings cause major changes in ocean circulation, marine productivity and temperature distribution during the termination that affect ocean sediments. In turn, the model simulates a substantial increase in pCO_2 ($\sim$7 ppmv) during the Holocene as a result of millennial-scale sediment adjustments. This is considerable compared to the overall Holocene variations of 20 ppmv. However, our estimate is uncertain as the reorganization of the carbon cycle during the termination is not well understood.

[59] Our results indicate a small but positive contribution to the Holocene pCO_2 increase from temperature-driven changes in the solubility of CO_2 during the Holocene. This is in contrast to *Brovkin et al.* [2008], who suggest a negative influence of temperature-related solubility changes on atmospheric CO_2. The global SST increase of 0.15°C obtained in the Bern3D is comparable to the one simulated by general circulation models (MIROC3.2 and CCSM). In addition, in agreement with proxies and other modeling studies, the Bern3D displays a slight cooling in the North Atlantic and the Southern Ocean and a warming at low latitudes [*Schneider et al.*, 2010].

[60] Major abrupt oceanic circulation reorganizations most likely occurred during the last termination in response to freshwater input from land ice sheets [*McManus et al.*, 2004; *Piotrowski et al.*, 2004; *Okazaki et al.*, 2010; *Menviel et al.*, 2011]. We find in agreement with earlier studies [*Marchal et al.*, 1998, 1999; *Obata*, 2007; *Menviel et al.*, 2008; *Schmittner and Galbraith*, 2008] that abrupt circulation changes, such as the recovery from the YD cold period ($\sim$11.6 ka B.P.), have an impact on atmospheric CO_2 and $\delta^{13}CO_2$. Particularly, oceanic reorganizations occurring during the ACR and the YD could play a role in shaping the

atmospheric CO_2 and $\delta^{13}CO_2$ variations during the period 11–9 ka B.P. (see auxiliary material).

[61] In agreement with the findings of *Ridgwell et al.* [2003] and *Kleinen et al.* [2010] our results indicate that coral reef growth and other shallow-water carbonate deposition are a major contributor for the atmospheric CO_2 rise after 7 ka B.P. However, in agreement with *Joos et al.* [2004], we find that the carbonate compensation mechanism due to land carbon uptake during the termination (18–11 ka B.P.) and the early Holocene also contributes significantly to the atmospheric CO_2 rise after 7 ka B.P. Carbonate compensation of earlier land uptake and carbonate deposition influence atmospheric CO_2 and $\delta^{13}CO_2$ in a similar way and the magnitude of these two processes can not be firmly distinguished from the atmospheric records. We find that a deglacial land carbon uptake as low as 90 GtC can still be reconciled with the atmospheric record and estimates of shallow water carbonate deposition when combining a land release during the termination with the Holocene reconstruction of *Elsig et al.* [2009] (Table 2 in Text S1 and Figure S5).

[62] As already suggested by *Elsig et al.* [2009], the main contributor to the atmospheric $\delta^{13}CO_2$ changes during the Holocene is the land carbon uptake/release from 11 to 0 ka B.P. *Elsig et al.* [2009] applied a mass balance approach only considering changes in land carbon and in the marine calcium carbonate cycle. The results from a broad range of factorial experiments with the mechanistic Bern3D model suggest that this simple approach is viable and quantitatively robust for the last 9 ka. Indeed, carbonate related processes have a relatively small but not negligible influence on atmospheric $\delta^{13}CO_2$ (Figure 1b). In addition, simulated changes in marine export productivity and SST during the Holocene are relatively small and thus have a negligible influence on atmospheric $\delta^{13}CO_2$.

[63] The terrestrial carbon uptake estimated by *Elsig et al.* [2009] between 11 and 5 ka B.P. (290 $\pm$ 36 GtC) is slightly higher than the range suggested by modeling studies (about 100 to 200 GtC) [*Kaplan et al.*, 2002; *Joos et al.*, 2004; *Menviel et al.*, 2011]. However, carbon uptake by northern peatlands, which has recently been identified as an important carbon sink during the deglaciation [*Yu et al.*, 2010; *Yu*, 2010], was not taken into account in these modeling studies. The Holocene terrestrial carbon balance may thus be closed in the following way. Radiocarbon data indicate that about half of the carbon on contemporary peatlands (150–275 GtC) [*Gorham*, 1991; *Tarnocai et al.*, 2009; *Yu et al.*, 2010] accumulated before 5 ka BP [*Yu et al.*, 2010], a quarter during the period 5 to 2 ka B.P. and the rest during the last two millennia. By definition, the data include only peatlands that still exist today and can not account for any potential carbon loss from peatlands that might have existed during earlier periods. Thus, the current peat carbon stock represents an upper-bound estimate of the net carbon flux into peats during the Holocene. Both scenarios used in this study (LOV-ELS and LOV2-YU) suggest a land carbon uptake of $\sim$290 GtC between 11 and 5 ka B.P., consistent with [*Yu*, 2010]. In addition, the combination of the lower bound shallow-water carbonate deposition (VEC) with the LOV-ELS scenario as well as the combination of the upper bound shallow-water carbonate deposition (R1) with the LOV2-YU scenario give a reasonable representation of the recorded atmospheric CO_2 and $\delta^{13}CO_2$ over the period 11–5 kaB.P.

[64] During the last 5 kyr, however, *Elsig et al.* [2009] suggests a land carbon release of 36 $\pm$ 37 GtC, while *Yu et al.* [2010] suggest a peat build up of about 190 GtC. The terrestrial carbon budget suggested by the ELS scenario for the last 5 kyr would indicate an approximate balance between peat uptake and carbon release from anthropogenic land use [*Stocker et al.*, 2011; *Olofsson and Hickler*, 2008; *Kaplan et al.*, 2010]. The combination of the lower bound shallow-water carbonate deposition (VEC) with the LOV-ELS scenario gives a reasonable fit with the atmospheric data recorded in ice cores. On the other hand, the combination of the upper bound shallow-water carbonate deposition (R1) with the LOV2-YU scenario during the last 5 kyr is difficult to reconcile with the proxy records. Indeed, while the high land carbon uptake suggested by *Yu et al.* [2010] is required to compensate for the strong atmospheric CO_2 increase generated by the shallow-water carbonate deposition scenario R1, the slope of the atmospheric $\delta^{13}CO_2$ is then much greater than in the ice record. As shown in section 3, both the high land carbon uptake and the high shallow-water carbonate deposition induce an increase in $\delta^{13}CO_2$.

[65] Results from this study would thus suggest that the atmospheric CO_2 and $\delta^{13}CO_2$ variations over the period 11–5 ka B.P. could be explained by a land carbon uptake of about 290 GtC and a shallow-water carbonate deposition of $0.15–0.4 \times 10^{17}$ molC. For the last 5 kyr, the combined VEC and ELS scenarios lead to a good agreement with the ice core records while this is not the case for the combined R1 and LOV2-YU scenario. Additional experiments (not shown) help to explore the possible range of shallow-water carbonate deposition and land carbon uptake for the last 5 kyr. Results indicate a probable shallow-water carbonate deposition for the last 5 kyr of $0.13–0.31 \times 10^{17}$ molC associated with a land carbon change of -35 GtC to +75 GtC. This equates to a total range of shallow-water carbonate deposition over the Holocene of $\sim 0.35–0.75 \times 10^{17}$ mol.

[66] A caveat is that a constant atmosphere-land isotopic fractionation factor is applied in the inverse approach by *Elsig et al.* [2009] and in this study, therefore not taking into account any relative changes in the occurrence of C3/C4 plants and other influences on fractionation. However, using the LPJ-DGVM vegetation model, *Joos et al.* [2004] found that changes in fractionation and C3/C4 plant abundance due to climate and CO_2 changes lead to a decrease in $\delta^{13}C$ signature of the terrestrial biosphere of about 0.5 permil from the early Holocene (10 ka B.P.) to pre-industrial times. A 0.5 permil decrease in biosphere $\delta^{13}C$ translates into an atmospheric $\delta^{13}C$ decrease of about 0.02 permil. This suggests that changes in the atmosphere-land isotopic fractionation have a small influence on the results presented above.

[67] Changes in the rate of weathering processes and volcanic CO_2 emissions have not been included here. The rate of changes of carbonate and silicate weathering from the LGM to pre-industrial times are highly uncertain and no consensus in the literature has emerged as to the direction of these changes [*Munhoven*, 2002; *Foster and Vance*, 2006; *Vance et al.*, 2009; *Lerman et al.*, 2011]. However, as most of the climatic and sea level changes occurred during the termination (18–11 ka B.P.), weathering changes during the Holocene should be quite small. An upper estimate [*Lerman*

et al., 2011] suggests an additional 0.1×10^{17} molC input to the coastal ocean by riverine flux during the Holocene. This additional DIC riverine input could counterbalance some of the DIC lost by shallow-water carbonate deposition. This would thus lead to a slightly higher range of possible shallow-water carbonate deposition during the Holocene than indicated above.

[68] *Huybers and Langmuir* [2009] proposed that volcanic emissions were 2 to 6 times above background levels between 12 and 7 ka B.P. According to their hypothesis, enhanced volcanism would increase atmospheric CO_2 by about 20 ppmv between 11 and 7 ka B.P. in contrast to the observed decrease of 5 ppmv. Such a scenario would require a much greater land carbon uptake than inferred from the ice core $\delta^{13}CO_2$ record to compensate for the volcanic CO_2 release. We conclude that the good agreement between simulated and reconstructed pCO_2 and $\delta^{13}CO_2$ for simulations driven with relatively well-established forcings leaves little room for a dominant role of volcanic CO_2 outgassing.

[69] We have shown in this study that the atmospheric CO_2 and $\delta^{13}CO_2$ variations during the Holocene result from the subtle combination of forcings and processes with different timescales and characteristics. Many different processes operating during the glacial termination and/or during the Holocene influence atmospheric CO_2. A more general implication is that the exact evolution of atmospheric CO_2 during interglacial periods depends on the precise balance of partly opposing processes with different temporal evolutions. It is thus expected that different warm periods with their own forcing characteristics and preceded by different glacial terminations show different evolutions of atmospheric CO_2 as evidenced by the ice core record [*Lüthi et al.*, 2008].

[70] **Acknowledgments.** We thank H. Fischer, J. Schmitt, O. Marchal as well as two anonymous reviewers for their helpful comments. This study received support by the Swiss National Science Foundation and by the European Commission through the FP7 projects Past4Future (grant 243908) and CARBOCHANGE (grant 264879). L. Menviel is supported by funding through the Oeschger Center for Climate Change. We acknowledge the international modeling groups for providing their data for analysis and the Laboratoire des Sciences du Climat et de l'Environnement (LSCE) for collecting and archiving the model data. The PMIP2/MOTIF Data Archive is supported by CEA, CNRS, the EU project MOTIF (EVK2-CT-2002-00153) and the Programme National d'Etude de la Dynamique du Climat (PNEDC). The analyses were performed using version 11-01-2007 of the database. More information is available on http://pmip2.lsce.ipsl.fr/and http://motif.lsce.ipsl.fr/.

References

Archer, D. E., H. Keshgi, and E. Maier-Reimer (1997), Multiple timescales for neutralization of fossil fuel CO_2, *Geophys. Res. Lett.*, *24*, 405–408.

Beerling, D. J. (1999), New estimates of carbon transfer to terrestrial ecosystems between the Last Glacial Maximum and the Holocene, *Terra Nova*, *11*, 162–167.

Berger, A. (1978), Long term variations of daily insolation and Quaternary climate change, *J. Atmos. Sci.*, *35*, 2362–2367.

Bickert, T., and A. Mackensen (2003), Last Glacial to Holocene changes in South Atlantic deep water circulation, in *The South Atlantic in the Late Quaternary: Reconstruction of Material Budgets and Current Systems*, pp. 671–695, Springer, Berlin.

Bickert, T., and G. Wefer (1996), Late Quaternary deep water circulation in the South Atlantic: Reconstruction from carbonate dissolution and benthic stable isotopes, in *The South Atlantic in the Late Quaternary: Present and Past Circulation*, pp. 599–620, Springer, Berlin.

Bird, M. I., J. Lloyd, and G. D. Farquhar (1994), Terrestrial carbon storage at the LGM, *Nature*, *371*, 566.

Boyle, E. A., and L. D. Keigwin (1985), Comparison of Atlantic and Pacific paleochemical records for the last 215,000 years: Changes in deep ocean circulation and chemical inventories, *Earth. Planet. Sci. Lett.*, *76*, 135–150.

Broecker, W. S., and T.-H. Peng (1987), The role of $CaCO_3$ compensation in the glacial to interglacial atmospheric CO_2 change, *Global Biogeochem. Cycles*, *1*, 15–39.

Broecker, W. S., J. Lynch-Stieglitz, E. Clark, I. Hajdas, and G. Bonani (2001), What caused the atmosphere's CO_2 content to rise during the last 8000 years?, *Geochem. Geophys. Geosyst.*, *2*, 1062, doi:10.1029/2001GC000177.

Brovkin, V., J. Bendtsen, M. Claussen, A. Ganopolski, C. Kubatzki, V. Petoukhov, and A. Andreev (2002), Carbon cycle, vegetation, and climate dynamics in the Holocene: Experiments with the CLIMBER-2 model, *Global Biogeochem. Cycles*, *16*(4), 1139, doi:10.1029/2001GB001662.

Brovkin, V., J.-H. Kim, M. Hofmann, and R. Schneider (2008), A lowering effect of reconstructed Holocene changes in sea surface temperatures on the atmospheric CO_2 concentration, *Global Biogeochem. Cycles*, *22*, GB1016, doi:10.1029/2006GB002885.

Carter, L., B. Manighetti, G. Ganssen, and L. Northcote (2008), Southwest Pacific modulation of abrupt climate change during the Antarctic Cold Reversal–Younger Dryas, *Palaeogeogr. Palaeoclimatol. Palaeoecol.*, *260*, 284–298.

Curry, W. B., J. C. Duplessy, L. Labeyrie, and N. J. Shackleton (1988), Changes in the distribution of $\delta^{13}C$ of deep water $\sum CO_2$ between the last glaciation and the Holocene, *Paleoceanography*, *3*, 317–341.

Doney, S. C., D. M. Glover, and R. G. Najjar (1996), A new coupled, one-dimensional biological-physical model for the upper ocean: Applications to the JGOFS Bermuda Atlantic time-series study (BATS) site 1, *Deep Sea Res., Part II*, *43*, 591–624.

Duplessy, J. C., N. J. Shackleton, R. G. Fairbanks, L. Labeyrie, D. Oppo, and N. Kallel (1988), Deepwater source variations during the last climate cycle and their impact on the global deepwater circulation, *Paleoceanography*, *3*, 343–360.

Dürkop, A., W. Hale, S. Mulitza, J. PLtzold, and G. Wefer (1997), Late Quaternary variations of sea surface salinity and temperature in the western tropical Atlantic: Evidence from δ18O of *Globigerinoides sacculifer*, *Paleoceanography*, *12*, 764–772.

Edwards, N. R., and R. Marsh (2005), Uncertainties due to transport-parameter sensitivity in an efficient 3-D ocean-climate model, *Clim. Dyn.*, *3*, 67–94.

Edwards, N. R., A. J. Willmot, and P. D. Killworth (1998), On the role of topography and wind stress on the stability of the thermohaline circulation, *J. Phys. Oceanogr.*, *28*, 756–778.

Elsig, J., J. Schmitt, D. Leuenberger, R. Schneider, M. Eyer, M. Leuenberger, F. Joos, H. Fischer, and T. F. Stocker (2009), Stable isotope constraints on Holocene carbon cycle changes from an Antarctic ice core, *Nature*, *461*, 507–510.

Fairbanks, R. G. (1989), A 17,000-year glacio-eustatic sea level record: Influence of glacial melting rates on the Younger Dryas event and deep-ocean circulation, *Nature*, *342*, 637–642.

Foster, G. L., and D. Vance (2006), Negligible glacial-interglacial variation in continental chemical weathering rates, *Nature*, *444*, 918–921.

Francois, L. M., C. Delire, P. Warnant, and G. Munhoven (1998), Modelling the glacial-interglacial changes in the continental biosphere, *Global Planet. Change*, *17*, 37–52.

Freeman, K. H., and J. M. Hayes (1992), Fractionation of carbon isotopes by phytoplankton and estimates of ancient CO_2 levels, *Global Biogeochem. Cycles*, *6*, 185–198.

Gehlen, M., L. Bopp, N. Emprin, O. Aumont, C. Heinze, and O. Ragueneau (2006), Reconciling surface ocean productivity, export fluxes and sediment composition in a global biogeochemical ocean model, *Biogeosciences*, *3*, 521–537.

Gorham, E. (1991), Northern peatlands: Role in the carbon cycle and probable responses to climatic warming, *Ecological App.*, *1*, 182–195.

Heinze, C., E. Maier-Reimer, A. M. E. Winguth, and D. Archer (1999), A global oceanic sediment model for long-term climate studies, *Global Biogeochem. Cycles*, *13*, 221–250.

Hodell, D. A., K. A. Venz, C. D. Charles, and U. S. Ninnemann (2003), Pleistocene vertical carbon isotope and carbonate gradients in the South Atlantic sector of the Southern Ocean, *Geochem. Geophys. Geosyst.*, *4*(1), 1004, doi:10.1029/2002GC000367.

Huybers, P., and C. Langmuir (2009), Feedback between deglaciation, volcanism, and atmospheric CO_2, *Earth Planet. Sci. Lett.*, *286*, 479–491.

Indermühle, A., et al. (1999), Holocene carbon cycle dynamics based on CO_2 trapped in ice at Taylor Dome, Antarctica, *Nature*, *398*, 121–126.

Jansen, E., et al. (2007), Paleoclimate, in *The Physical Science Basis. Contribution of Working Group I to the Fourth Assessment Report of the Intergovernmental Panel on Climate Change*, chap. 6, pp. 433–497, Cambridge Univ. Press, Cambridge, U. K.

Jin, X., N. Gruber, J. P. Dunne, J. L. Sarmiento, and R. A. Armstrong (2006), Diagnosing the contribution of phytoplankton functional groups to the production and export of particulate organic carbon, $CaCO_3$, and opal from global nutrient and alkalinity distributions, *Global Biogeochem. Cycles*, *20*, GB2015, doi:10.1029/2005GB002532.

Joos, F., and M. Bruno (1996), Pulse response functions are cost-efficient tools to model the link between carbon emissions, atmospheric CO_2 and global, *Phys. Chem. Earth*, *21*, 471–476.

Joos, F., S. Gerber, I. C. Prentice, B. L. Otto-Bliesner, and P. J. Valdes (2004), Transient simulations of Holocene atmospheric carbon dioxide and terrestrial carbon since the Last Glacial Maximum, *Global Biogeochem. Cycles*, *18*, GB2002, doi:10.1029/2003GB002156.

Kaplan, J. O., I. C. Prentice, W. Knorr, and P. J. Valdes (2002), Modeling the dynamics of the terrestrial carbon storage since the Last Glacial Maximum, *Geophys. Res. Lett.*, *29*(22), 2074, doi:10.1029/2002GL015230.

Kaplan, J. O., K. Krumhardt, E. C. Ellis, and W. F. Ruddiman (2010), Holocene carbon emissions as a result of anthropogenic land cover change, *Holocene*, *21*, 775–791, doi:10.1177/0959683610386983.

Keir, R. S. (1988), On the Late Pleistocene oean geochemistry and circulation, *Paleoceanography*, *3*, 413–445.

Keir, R. S., and W. H. Berger (1985), Late Holocene carbonate dissolution in the equatorial Pacific: Reef growth or neoglaciation?, in *The Carbon Cycle and Atmospheric CO_2: Natural Variations, Archean to Present*, *Geophys. Monogr. Ser.*, vol. 32, pp. 208–219, AGU, Washington, D. C.

Kim, J.-H., and R. R. Schneider (2004), GHOST global database for alkenone-derived Holocene sea-surface temperature records, http://doi.pangaea.de/10.1594/PANGAEA.761700, PANGAEA, Network for Geol. and Environ. Data, Germany.

Kim, J.-H., N. Rimbu, S. J. Lorenz, G. Lohmann, S. I. Nam, S. Schouten, C. Ruhlemann, and R. R. Schneider (2004), North Pacific and North Atlantic sea-surface temperature variability during the Holocene, *Quat. Sci. Rev.*, *23*, 2141–2154.

Kleinen, T., V. Brovkin, W. von Bloh, D. Archer, and G. Munhoven (2010), Holocene carbon cycle dynamics, *Geophys. Res. Lett.*, *37*, L02705, doi:10.1029/2009GL041391.

Kleypas, J. A. (1997), Modeled estimates of global reef habitat and carbonate production since the Last Glacial Maximum, *Paleoceanography*, *12*, 533–545.

Krakauer, N. Y., J. T. Randerson, F. W. Primeau, N. Gruber, and D. Menemenlis (2006), Carbon isotope evidence for the latitudinal distribution and wind speed dependence of the air-sea gas transfer velocity, *Tellus, Ser. B*, *58*, 390–417.

Labeyrie, L. D., J. C. Duplessy, and P. L. Blanc (1987), Variations in mode of formation and temperature of oceanic deep waters over the past 125,000 years, *Nature*, *327*, 477–482.

Lerman, A., M. Guidry, A. J. Andersson, and F. T. Mackenzie (2011), Coastal ocean Last Glacial Maximum to 2100 CO_2-carbonic acid-carbonate system: A modeling approach, *Aquat. Geochem.*, *17*, 749–773, doi:10.1007/s10498–011–9146–z.

Lisiecki, L. E., and M. E. Raymo (2005), A Pliocene-Pleistocene stack of 57 globally distributed benthic δ18O records, *Paleoceanography*, *20*, PA1003, doi:10.1029/2004PA001071.

Loulergue, L., A. Schilt, R. Spahni, V. Masson-Delmotte, T. Blunier, B. Lemieux, J.-M. Barnola, D. Raynaud, T. F. Stocker, and J. Chappellaz (2008), Orbital and millennial-scale features of atmospheric CH_4 over the past 800,000 years, *Nature*, *453*, 383–386.

Lüthi, D., et al. (2008), High-resolution carbon dioxide concentration record 650,000–800,000 years before present, *Nature*, *453*, 379–382, doi:10.1038/nature06949

Maier-Reimer, E., I. Kriest, J. Segschneider, and P. Wetzel (2005), The hamburg ocean carbon cycle model HAMOCC5.1.-Technical description release 1.1, *Tech. Rep. 14*, Max Planck Inst. for Meteorol., Hamburg, Germany.

Marchal, O., T. F. Stocker, and F. Joos (1998), Impact of oceanic reorganizations on the ocean carbon cycle and atmospheric carbon dioxide content, *Paleoceanography*, *13*, 225–244.

Marchal, O., T. F. Stocker, F. Joos, A. Indermühle, T. Blunier, and J. Tschumi (1999), Modelling the concentration of atmospheric CO_2 during the Younger Dryas climate event, *Clim. Dyn.*, *15*, 341–354.

Martrat, B., J. O. Grimalt, N. J. Shackleton, L. de Abreu, M. A. Hutterli, and T. F. Stocker (2007), Four climate cycles of recurring deep and surface water destabilizations on the Iberian margin, *Science*, *317*, 502–507.

McCave, I. N., L. Carter, and I. R. Hall (2008), Glacial-interglacial changes in water mass structure and flow in the SW Pacific Ocean, *Quat. Sci. Rev.*, *27*, 1886–1908.

McManus, J. F., R. Francois, J. M. Gherardi, L. D. Keigwin, and S. Brown-Leger (2004), Collapse and rapid resumption of Atlantic meridional circulation linked to deglacial climate changes, *Nature*, *428*, 834–837.

Menviel, L., A. Timmermann, A. Mouchet, and O. Timm (2008), Climate and marine carbon cycle response to changes in the strength of the Southern Hemispheric westerlies, *Paleoceanography*, *23*, PA4201, doi:10.1029/2008PA001604.

Menviel, L., A. Timmermann, O. Timm, and A. Mouchet (2011), Deconstructing the Last Glacial termination: The role of millennial and orbital-scale forcings, *Quat. Sci. Rev.*, *30*, 1155–1172.

Milliman, J. D. (1993), Production and accumulation of calcium carbonate in the ocean: Budget of a nonsteady state, *Global Biogeochem. Cycles*, *7*, 927–957.

Mix, A. C., and R. G. Fairbanks (1985), North Atlantic surface-ocean control of Pleistocene deep-ocean circulation, *Earth Planet. Sci. Lett.*, *73*, 231–243.

Mix, A. C., N. G. Pisias, R. Zahn, W. Rugh, C. Lopez, and K. Nelson (1991), Carbon 13 in Pacific deep and intermediate waters, 0–370 ka: Implications for ocean circulation and Pleistocene CO_2, *Paleoceanography*, *6*, 205–226.

Mollenhauer, G., R. R. Schneider, P. J. Müller, V. Spiess, and G. Wefer (2002), Glacial/interglacial variability in the Benguela upwelling system: Spatial distribution and budgets of organic carbon accumulation, *Global Biogeochem. Cycles*, *16*(4), 1134, doi:10.1029/2001GB001488.

Monnin, E., A. Indermühle, A. Dällenbach, J. Flückiger, B. Stauffer, T. F. Stocker, D. Raynaud, and J.-M. Barnola (2001), Atmospheric CO_2 concentration over the Last Glacial termination, *Science*, *291*, 112–114.

Montaggioni, L. F. (1988), Holocene reef growth history in mid-plate high volcanic islands, in *Proceedings of the 6th International Coral Reef Symposium*, vol. 3, pp. 455–460, Springer, Berlin.

Montenegro, A., M. Eby, J. O. Kaplan, K. J. Meissner, and A. J. Weaver (2006), Carbon storage on exposed continental shelves during the glacial-interglacial transition, *Geophys. Res. Lett.*, *33*, L08703, doi:10.1029/2005GL025480.

Mook, W. G. (1988), ^{13}C in atmospheric CO_2, *Neth. J. Sea Res.*, *20*, 211–223.

Mulitza, S. (1998), Stable isotopes of sediment core GeoB1523–2, http://doi.pangaea.de/10.1594/PANGAEA.53546, PANGAEA, Network for Geol. and Environ. Data, Germany.

Müller, S. A., F. Joos, N. R. Edwards, and T. F. Stocker (2006), Water mass distribution and ventilation time scales in a cost-efficient three-dimensional ocean model, *J. Climate*, *19*, 5479–5499.

Munhoven, G. (2002), Glacial-interglacial changes of continental weathering: Estimates of the related CO_2 and HCO_3^- flux variations and their uncertainties, *Glob. Planet. Change*, *33*, 155–176.

Najjar, R. G., J. Orr, C. L. Sabine, and F. Joos (1999), Biotic-HOWTO, internal OCMIP report, LSCE/CEA Saclay, Gif-sur-Yvette, France.

Obata, A. (2007), Climate-carbon cycle model response to freshwater discharge into the North Atlantic, *J. Climate*, *20*, 5962–5976.

Okazaki, Y., A. Timmermann, L. Menviel, N. Harada, A. Abe-Ouchi, M. Chikamoto, A. Mouchet, and H. Asahi (2010), Deep water formation in the North Pacific during the Last Glacial Termination, *Science*, *329*, 200–204.

Oliver, K. I. C., B. A. A. Hoogakker, S. Crowhurst, G. M. Henderson, R. E. M. Rickaby, N. R. Edwards, and H. Elderfield (2010), A synthesis of marine sediment core δ^{13}C data over the last 150,000 years, *Clim. Past*, *6*, 645–673.

Olofsson, J., and T. Hickler (2008), Effects of human land-use on the global carbon cycle during the last 6000 years, *Veget. Hist. Archaeobotany*, *17*, 605–615, doi:10.1007/s00334–007–0126–6.

Opdyke, B. N. (2000), Shallow water carbonate deposition and its effect on the carbon cycle, in *The Carbon Cycle*, pp. 161–168, Natl. Cent. for Atmos. Res., Boulder, Colo.

Oppo, D. W., and R. G. Fairbanks (1987), Variability in the deep and intermediate water circulation of the Atlantic Ocean during the past 25,000 years: Northern hemisphere modulation of the Southern Ocean, *Earth Planet. Sci. Lett.*, *86*, 1–15.

Orr, J., and R. G. Najjar (1999), Abiotic-HOWTO, internal OCMIP report, LSCE/CEA Saclay, Gif-sur-Yvette, France.

Pailler, D., and E. Bard (2002), High frequency palaeoceanographic changes during the past 140,000 yr recorded by the organic matter in sediments of the Iberian Margin, *Palaeogeogr. Palaeoclimatol. Palaeoecol.*, *181*, 431–452.

Parekh, P., F. Joos, and S. A. Müller (2008), A modeling assessment of the interplay between aeolian iron fluxes and iron-binding ligands in controlling carbon dioxide fluctuations during Antarctic warm events, *Paleoceanography*, *23*, PA4202, doi:10.1029/2007PA001531.

Peltier, W. R. (1994), Ice-age paleotopography, *Science*, *265*, 195–201.

Peltier, W. R. (2004), Global glacial isostasy and the surface of the ice-age Earth: The ICE-5G (VM2) model and GRACE, *Annu. Rev. Earth Planet Sci.*, *23*, 335–357.

Piotrowski, A. M., S. L. Goldstein, S. R. Hemming, and R. G. Fairbanks (2004), Intensification and variability of ocean thermohaline circulation through the last deglaciation, *Earth Planet. Sci. Lett.*, *225*, 205–220.

Ridgwell, A. J., A. J. Watson, M. A. Maslin, and J. O. Kaplan (2003), Implications of the coral reef buildup for the controls on atmospheric CO_2 since the Last Glacial Maximum, *Paleoceanography*, *18*(4), 1083, doi:10.1029/2003PA000893.

Ritz, S. P., T. F. Stocker, and F. Joos (2011), A coupled dynamical ocean–Energy balance atmosphere model for paleoclimate studies, *J. Climate*, *24*, 349–375.

Ryan, D. A., B. N. Opdyke, and J. S. Hell (2001), Holocene sediments of wistari reef: Towards a global quantification of coral reef related neritic sedimentation in the Holocene, *Palaeogeogr. Palaeoclimatol. Palaeoecol.*, *175*, 173–184.

Schmiedl, G., and A. Mackensen (1997), Late Quaternary paleoproductivity and deep water circulation in the eastern South Altantic Ocean: Evidence from benthic foraminifera, *Palaeogeogr. Palaeoclimatol. Palaeoecol.*, *130*, 43–80.

Schmittner, A., and E. D. Galbraith (2008), Glacial greenhouse-gas fluctuations controlled by ocean circulation changes, *Nature*, *456*, 373–376.

Schneider, B., G. Leduc, and W. Park (2010), Disentangling seasonal signals in Holocene climate trends by satellite-model-proxy integration, *Paleoceanography*, *25*, PA4217, doi:10.1029/2009PA001893.

Schurgers, G., U. Mikolajewicz, M. Gröger, E. Maier-Reimer, M. Vizcano, and A. Winguth (2006), Dynamics of the terrestrial biosphere, climate and atmospheric CO_2 concentration during interglacials: A comparison between Eemian and Holocene, *Clim. Past*, *2*, 205–220.

Shackleton, N. J. (1977), Carbon-13 in Uvigerina: Tropical rainforest history and the equatorial Pacific carbonate dissolution cycle, in *The Fate of Fossil Fuel CO_2 in the Oceans*, pp. 401–427, Plenum, New York.

Siegenthaler, U., and K. O. Muennich (1981), Carbon-13/carbon-12 fractionation during carbon dioxide transfer from air to sea, in *SCORE 16: Carbon Cycle Modelling*, pp. 249–257, Wiley, Chichester, U. K.

Siegenthaler, U., and H. Oeschger (1987), Biospheric CO_2 emissions during the past 200 years reconstructed by convolution of ice core data, *Tellus Ser. B*, *39*, 140–154.

Spalding, M. D., C. Ravilious, and E. P. Green (2001), *World Atlas of Coral Reefs*, Univ. of Calif. Press, Berkeley.

Stocker, B., K. Strassmann, and F. Joos (2011), Sensitivity of Holocene atmospheric CO_2 and the modern carbon budget to early human land use: Analyses with a process-based model, *Biogeosciences*, *8*, 69–88.

Tarnocai, C., J. G. Canadell, E. A. G. Schuur, P. Kuhry, G. Mazhitova, and S. Zimov (2009), Soil organic carbon pools in the northern circumpolar permafrost region, *Global Biogeochem. Cycles*, *23*, GB2023, doi:10.1029/2008GB003327.

Tschumi, T., F. Joos, and P. Parekh (2008), How important are Southern Hemisphere wind changes for low glacial carbon dioxide? A model study, *Paleoceanography*, *23*, PA4208, doi:10.1029/2008PA001592.

Tschumi, T., F. Joos, M. Gehlen, and C. Heinze (2011), Deep ocean ventilation, carbon isotopes, marine sedimentation and the deglacial CO_2 rise, *Clim. Past*, *7*, 771–800.

Vance, D., D. A. H. Teagle, and G. L. Foster (2009), Variable Quaternary chemical weathering fluxes and imbalances in marine geochemical budgets, *Nature*, *458*, 493–496.

Vecsei, A. (2004), A new estimate of global reefal carbonate production including the fore-reefs, *Global Planet. Change*, *43*, 1–18.

Vecsei, A., and W. H. Berger (2004), Increase of atmospheric CO_2 during deglaciation: Constraints on the coral reef hypothesis from patterns of deposition, *Global Biogeochem. Cycles*, *18*, GB1035, doi:10.1029/2003GB002147.

Walker, J. C. G., and B. C. Opdyke (1995), Influence of variable rates of neritic carbonate deposition on atmospheric carbon dioxide and pelagic sediment, *Paleoceanography*, *10*, 415–427.

Wang, Y., L. A. Mysak, and N. T. Roulet (2005), Holocene climate and carbon cycle dynamics: Experiments with the "green" McGill Paleoclimate Model, *Global Biogeochem. Cycles*, *19*, GB3022, doi:10.1029/2005GB002484.

Wang, Y., N. T. Roulet, S. Frolking, and L. A. Mysak (2009), The importance of Northern Peatlands in global carbon systems during the Holocene, *Clim. Past*, *5*, 683–693.

Wei, G., C. Wang, M. Lee, and K. Wei (2006), High-resolution benthic foraminifer $\delta^{13}C$ records in the South China Sea during the last 150 ka, *Mar. Geol.*, *232*, 227–235.

Yu, J., W. S. Broecker, H. Elderfield, Z. Jin, J. McManus, and F. Zhang (2010a), Loss of carbon from the deep sea since the Last Glacial Maximum, *Science*, *330*, 1084–1087.

Yu, J., G. L. Foster, H. Elderfield, W. S. Broecker, and E. Clark (2010b), An evaluation of benthic foraminiferal b/ca and $\delta^{11}b$ for deep ocean carbonate ion and ph reconstructions, *Earth Planet. Sci. Lett.*, *293*, 114–120.

Yu, Z. (2010), Holocene carbon flux histories of the world's peatlands: Global carbon-cycle implications, *Holocene*, *21*, 761–774, doi:10.1177/0959683610386982.

Yu, Z., J. Loisel, D. P. Brosseau, D. W. Beilman, and S. J. Hunt (2010), Global peatland dynamics since the Last Glacial Maximum, *Geophys. Res. Lett.*, *37*, L13402, doi:10.1029/2010GL043584.

Zeng, N. (2003), Glacial-interglacial atmospheric CO_2 changes–The glacial burial hypothesis, *Adv. Atmos. Sci.*, *20*, 677–693.

Zimov, N. S., S. A. Zimov, A. E. Zimova, G. M. Zimova, V. I. Chuprynin, and F. S. Chapin III (2009), Carbon storage in permafrost and soils of the mammoth tundra-steppe biome: Role in the global carbon budget, *Geophys. Res. Lett.*, *36*, L02502, doi:10.1029/2008GL036332.

F. Joos and L. Menviel, Oeschger Centre for Climate Change Research, University of Bern, Sidlerstrasse 5, CH-3012 Bern, Switzerland. (menviel@climate.unibe.ch)